

1 **TITLE: IGF2 is up-regulated by epigenetic mechanisms in hepatocellular**
2 **carcinoma and is an actionable oncogene in experimental models**

3 **SHORT-TITLE : IGF2 as key target for HCC therapy**

4

5 **Authors:** Iris Martinez-Quetglas¹, Roser Pinyol¹, Daniel Dauch², Sara Torrecilla¹, Victoria
6 Tovar¹, Agrin Moeini¹, Clara Alsinet¹, Anna Portela³, Leonardo Rodriguez-Carunchio¹,
7 Manel Solé¹, Amaia Lujambio^{4,5}, Augusto Villanueva^{4,6}, Swan Thung⁴, Manel Esteller^{3,7},
8 Lars Zender^{2,8}, Josep M. Llovet^{1,4,7}.

9 **Affiliations:**

10 ¹Liver Cancer Translational Research Laboratory, Barcelona Clinic Liver Cancer Group
11 (BCLC), Liver Unit, IDIBAPS-Hospital Clínic de Barcelona, CIBERehd Universitat de
12 Barcelona, Catalonia, Spain.

13 ²Division of Translational Gastrointestinal Oncology, Department of Internal Medicine I,
14 University of Tuebingen, Tuebingen, Germany.

15 ³Cancer Epigenetics and Biology Program, Bellvitge Biomedical Research Institute
16 (IDIBELL), Barcelona, Catalonia, Spain.

17 ⁴ Liver Cancer Program, Division of Liver Diseases and Pathology Department, Tisch
18 Cancer Institute, Department of Medicine, Icahn School of Medicine at Mount Sinai, New
19 York, NY, USA.

20 ⁵Oncological Sciences Department, Icahn School of Medicine at Mount Sinai, New York,
21 NY 10029, USA.

22 ⁶Division of Hematology and Medical Oncology, Department of Medicine, Icahn School of
23 Medicine at Mount Sinai, New York, NY, USA.

24 ⁷Institució Catalana de Recerca i Estudis Avançats (ICREA), Barcelona, Catalonia, Spain.

25 ⁸Translational Gastrointestinal Oncology Group within the German Center for Translational
26 Cancer Research (DKTK), German Cancer Research Center (DKFZ), Heidelberg, Germany

27 **Grant support:** JML is supported by grants from the European Commission (HEPTROMIC,
28 proposal number 259744; HEPCAR, proposal number 667273-2), The Samuel Waxman
29 Cancer Research Foundation, the Spanish Ministry of Economy and Competitiveness
30 (SAF2013-41027-R), the Asociación Española Contra el Cáncer (AECC) and the Tisch
31 Cancer Institute at Mount Sinai (P30 CA196521). ME is funded by Cellex Foundation, Botin
32 Foundation, Health and Science Departments of the Catalan Government (Generalitat de
33 Catalunya). AL is supported by the AASLD Pinnacle Research Award. AV is supported by the
34 AASLDF Alan Hofmann Clinical and Translational Research Award. LZ is supported by the
35 German Research Foundation, DFG (Emmy Noether Programme ZE 545/2-1 to L.Z.,
36 Gottfried Wilhelm Leibniz Program and SFB685), the Helmholtz Association the European
37 Research Council. IM-Q, RP, ST, VT and AM are funded by CIBERehd, AECC, the Spanish
38 Ministry of Economy and Competitiveness and European Commission.

39 **Author contribution:** IMQ (study concept and design; acquisition of data; analysis and
40 interpretation of data; drafting of the manuscript; statistical analysis), RP (study concept and
41 design; acquisition of data; analysis and interpretation of data; critical revision of the
42 manuscript for important intellectual content; statistical analysis; study supervision), DD

43 (acquisition of data; analysis and interpretation of data; critical revision of the manuscript for
44 important intellectual content; statistical analysis), ST (acquisition of data; analysis and
45 interpretation of data; technical, support); VT (acquisition of data; analysis and interpretation
46 of data; technical support; study supervision); AM (acquisition of data; study concept and
47 design); LRC (analysis and interpretation of data); CA (study concept and design; critical
48 revision of the manuscript for important intellectual content); SB (acquisition of data;
49 technical support); AP (acquisition of data; analysis and interpretation of data); MS (analysis
50 and interpretation of data); AL (critical revision of the manuscript for important intellectual
51 content); AV (critical revision of the manuscript for important intellectual content); ME
52 (critical revision of the manuscript for important intellectual content); LZ (critical revision of
53 the manuscript for important intellectual content); JML (study concept and design; critical
54 revision of the manuscript for important intellectual content; obtained funding; study
55 supervision).

56 **Abbreviation list:**

57 AKT: protein kinase B
58 Akt1: gene encoding for AKT
59 BrdU: Bromodeoxyuridine
60 CD31: cluster of differentiation 31
61 EPCAM: Epithelial cell adhesion molecule
62 FC: fold change
63 GEMM: genetically-engineered mouse model
64 GSEA: Gene Set Enrichment Analysis
65 IGF: insulin-like growth factor

66	IGF1/2:	insulin-like growth factor 1 and 2
67	IGF2:	insulin-like growth factor 2
68	INSR:	insulin receptor
69	INSR-A:	insulin receptor, isoform A
70	INSR-B:	insulin receptor, isoform B
71	IPA:	Ingenuity Pathway Analysis
72	KRT19:	Keratin, type I cytoskeletal 19
73	LOI:	loss of imprinting
74	mAb:	monoclonal antibody
75	miRNA:	micro-RNA
76	P1, P2, P3 and P4:	promoters 1, 2, 3 and 4
77	SALL4:	Sal-like protein 4
78	sh:	short hairpin
79	TKI:	tyrosine kinase inhibitors
80	VEGFA:	Vascular endothelial growth factor A

81

82 **Correspondence:** Josep M. Llovet; Liver Cancer Translational Research Laboratory,
83 Barcelona Clinic Liver Cancer Group (BCLC), IDIBAPS-Hospital Clinic, Rosselló 153,
84 08039, Barcelona, Catalonia, Spain; Tel. 0034-932.279.155; Email address:
85 jmllovet@clinic.cat

86 **Disclosures:** Boehringer Ingelheim supported the *in vitro* part of the study with a research
87 grant. JML is a consultant for Boehringer Ingelheim.

88 **Transcript-Profiling:** Microarray data were deposited in Gene Expression Omnibus
89 database with the accession numbers GSE63898, GSE56588, GSE74618 and GSE85274.

90 **Abstract**

91 **Background & Aims:** Effective treatments are urgently needed for hepatocellular
92 carcinoma (HCC), which is usually diagnosed at advanced stages. Signaling via the insulin-
93 like growth factor (IGF) pathway is aberrantly activated in HCC by IGF2 overexpression.
94 We aimed to elucidate the mechanism of IGF2 overexpression and its oncogenic activities,
95 and evaluate the anti-tumor effects of reducing IGF2 signaling.

96 **Methods:** We obtained 228 HCC samples from patients who underwent liver resection,
97 168 paired non-tumor adjacent cirrhotic liver samples, and 10 non-tumor liver tissues from
98 patients undergoing resection for hepatic hemangioma. We analyzed gene expression,
99 micro RNA (miRNA), and DNA methylation profiles for all samples, focusing on genes in
100 the IGF signaling pathway. IGF2 was expressed in SNU449 and PLC5 HCC cells and
101 knocked down with small hairpin RNAs in Hep3B and Huh7 cell lines. We analyzed these
102 cells for proliferation, apoptosis, migration, and colony formation. We performed studies of
103 mice engineered to express Myc and Akt1 in liver, which develop liver tumors, with or
104 without hepatic expression of IGF2. Mice with xenograft tumors grown from HCC cells
105 were administered with a monoclonal antibody against IGF1 and IGF2 (BI 836845), along
106 with sorafenib; tumor growth was measured and tissues were analyzed by
107 immunohistochemistry and immunoblots.

108 **Results:** Levels of IGF2 mRNA and protein were increased more than 20-fold in 15% of
109 human HCC tissues, compared with non-tumor liver tissues. Methylation at the fetal
110 promoters of *IGF2* was reduced in the HCC samples and cell lines that overexpressed
111 IGF2, compared with those that did not overexpress IGF2 and non-tumor tissues. Tumors
112 that overexpressed IGF2 had gene expression patterns significantly associated with hepatic

113 progenitor cell features, stellate cell activation, NOTCH signaling and an aggressive
114 phenotype ($P<.0001$). In mice engineered to express *Myc* and *Akt1* in liver, co-expression
115 of *Igf2* accelerated formation of liver tumors, compared to mice with livers expressing only
116 *Myc* and *Akt1*, and shortened survival times ($P=.02$). The antibody BI 836845 blocked
117 phosphorylation of IGF1 receptor (IGF1R) in HCC cell lines and reduced their proliferation
118 and colony formation. In mice with xenograft tumors, injection of BI 836845, with or
119 without sorafenib, slowed tumor growth and increased survival times compared to vehicle
120 or sorafenib alone. BI 836845 inhibited phosphorylation of IGF1R and AKT and reduced
121 decreased tumor vascularization, compared with vehicle.

122 **Conclusions:** A large proportion of HCC samples were found to overexpress IGF2, via
123 demethylation of its fetal promoter. Overexpression of IGF2 accelerates formation of liver
124 tumors in mice with hepatic expression of MYC and AKT1, via activation of IGF1R
125 signaling. An antibody against IGF1 and IGF2 slows growth of xenograft tumors and
126 increases survival of these mice.

127 **Keywords:** mouse model, hepatocarcinogenesis, IGF receptor, epigenetic modification

128 **Background**

129 Liver cancer is the second cause of cancer-related death worldwide and has an incidence of
130 850,000 new cases per year, thus representing a major public health problem¹.
131 Hepatocellular carcinoma (HCC) is the most common type of liver cancer ranking as the
132 16th cause of death globally ¹. Although surveillance programs for high-risk patients have
133 been implemented during the past decade, most patients are still diagnosed at advanced
134 stages. The only approved systemic therapy for these patients is sorafenib, which extends
135 survival from 8 to 11 months ². Seven additional targeted therapies tested in phase III trials
136 in first and second line have failed to improve survival ^{3,4}. Among the reasons for these
137 unsatisfactory results are the suboptimal understanding of the HCC critical drivers and the
138 lack of biomarker-based studies ^{3,4}. Thus, the identification of novel molecular targets and
139 therapies is an unmet medical need in HCC ³.

140 Over the past decade, comprehensive sequencing efforts have established the landscape of
141 gene mutations, chromosomal aberrations and epigenetic alterations that characterize
142 different cancer types, including HCC⁵⁻⁹. The oncogenic consequences of various structural
143 alterations have been extensively validated ^{3,5}; however, the role of genes altered by
144 epigenetic mechanisms (epi-drivers ⁹) has not been fully elucidated in HCC ^{3,7,10}. Similar to
145 other cancers ^{11,12}, the identification of actionable epi-drivers could provide novel treatment
146 options for the clinical management of this malignancy.

147 The IGF (insulin-like growth factor) signaling is frequently altered in HCC and constitutes a
148 promising therapeutic target ^{13,14}. Earlier studies pointed to IGF1R (insulin-like growth factor
149 1 receptor) as a potential oncogene ¹³; however, subsequent clinical trials blocking this

150 target by means of IGF1R monoclonal antibodies (mAb) or IGF1R/INSR (insulin receptor)
151 tyrosine kinase inhibitors (TKI) failed to demonstrate beneficial outcomes ¹⁵. Alternative
152 therapeutic strategies to inhibit IGF-pathway activation have been designed. For example,
153 BI 836845 is a mAb that abrogates IGF signaling and the pro-proliferative isoform INSR-A
154 by neutralizing IGF1 and 2 without affecting insulin metabolic functions through INSR-B
155 ¹⁶. IGF2 is highly overexpressed in HCC ^{13,14}, and could be a potential driver in
156 hepatocarcinogenesis. *IGF2* is a paternally imprinted growth factor regulated by four
157 different promoters. In the human liver, *IGF2* is monoallelically expressed during fetal
158 stages from three promoters (P2, P3 and P4) and in adults from both alleles of promoter P1
159 ¹⁷. The upregulation of *IGF2* observed in HCC can be partially explained by the
160 reactivation of *IGF2* transcription from the fetal-specific promoters ¹³. However, further
161 studies are needed to elucidate the precise mechanisms of deregulation of *IGF2* in HCC,
162 the specific contribution of *IGF2* overexpression to HCC development and its potential as a
163 therapeutic target.

164 In this study, we describe an epigenetic mechanism responsible for the reactivation of *IGF2*
165 fetal promoters in HCC and the association of these tumors with hepatic-progenitor cell
166 features. Moreover, we define the contribution of *IGF2* to the development of
167 hepatocarcinogenesis in genetically engineered mouse models (GEMM), and demonstrate
168 the *in vitro* and *in vivo* antioncogenic efficacy of IGF1/2-mAb through the reduction of cell
169 proliferation and angiogenesis. Taken together, we identify an actionable epi-driver in HCC
170 and a subset of patients that could benefit from anti-IGF2 therapy.

171 **Materials and Methods**

172 **Human tissue samples**

173 Human samples were collected following Institutional Review Board (Hospital Clinic de
174 Barcelona) and patient written informed consent. The study included samples from the
175 Heptronic Consortium used in previous studies ⁷: 228 HCC tumor samples from patients
176 who underwent liver resection, 168 paired non-tumor liver adjacent cirrhotic tissue samples
177 and 10 normal liver samples obtained from patients undergoing resection for hepatic
178 hemangioma. Samples were collected from three institutions of the HCC Genomic
179 Consortium (IRCCS Istituto Nazionale Tumori-Milan, Hospital Clínic-Barcelona and
180 Mount Sinai-New York). **Table S1** presents the main clinico-pathological features of the
181 patients included in the study.

182 **Chemically-induced mouse model of HCC**

183 All protocols involving animals were approved by the Institutional Animal Use and Care
184 Committee from the University of Barcelona. The induction of hepatic fibrosis and HCC
185 was based on a recently established model ¹⁸, and recapitulates the physiologic, histological
186 and molecular features of fibrosis, cirrhosis and HCC. Briefly, 15-days-old C57BL/6 male
187 mice ($n = 10$) received a single intraperitoneal injection of the hepatocarcinogen
188 diethylnitrosamine (DEN) (25 mg/kg dissolved in 0.9% of sodium chloride). At 4 weeks of
189 age, mice received a weekly intraperitoneal administration of the hepatotoxin carbon
190 tetrachloride (CCl₄) diluted in corn oil at a dosage 0.5 µl/g for 11-14 weeks. Control mice
191 ($n = 9$) received the vehicles of DEN and CCl₄. Livers were removed from the mice at 18
192 weeks of age and stored at -80 °C for RNA extraction.

193 **Genetically engineered mosaic mouse models**

194 Hydrodynamic tail vein injection was described recently¹⁹⁻²¹. Mice (four to six weeks old)
195 received 25 µg of transposon plasmids and 5 µg of transposase (Sleeping Beauty 13;
196 SB13). *SB13*, transposons encoding for *Myc* and *Akt1* and empty transposon plasmids were
197 previously described^{19,21}. The *Igf2* transposon plasmid was generated by PCR cloning, the
198 *Igf2* cDNA was obtained from Open Biosystems, while p19^{Arf^{-/-}} mice (male C57BL/6
199 background) were provided by Scott W. Lowe (Memorial Sloan Kettering Cancer Center,
200 New York, New York, USA). These mice were generated by Charles Sherr (St. Jude
201 Children's Research Hospital, Memphis, Tennessee, USA). C57BL/6 wildtype male mice
202 were obtained from Harlan (Rossdorf, Germany). DNA for hydrodynamic tail vein
203 injection was generated using the Qiagen EndoFreeMaxi Kit. The DNA was diluted in 0.9%
204 NaCl and injected at a volume of 10% of mouse body weight.

205 **Human HCC subcutaneous xenograft mouse model**

206 Ten million Hep3B cells were subcutaneously injected in a ratio 1:1 with matrigel
207 (Corning, Christiansburg, VA) into the right flank of NOD/SCID 6-8 weeks old female
208 mice (Harlan). Tumor size was measured three times per week using a hand calliper and
209 tumor volume was calculated using the following equation: (width² x length)/2. Animals
210 were randomized once tumor volume reached 100-200 mm³ into four arms: a) sorafenib (*n*
211 = 12), b) IGF1/2-mAb (*n* = 12), c) combination (sorafenib + IGF1/2-mAb, *n* = 13) and d)
212 vehicle (drug vehicles, *n* = 8). Mice randomization was performed using the Random
213 number generator module from Graph Pad software (San Diego, USA). Sorafenib was
214 dissolved in ethanol 95%/cremophor/sterile water (12.5:12.5:75) and administered orally at

215 15 mg/kg/day dosage²². The IGF1/2-mAb (BI 836845) was injected once weekly
216 intraperitoneally at 200 mg/kg according to provider recommendations¹⁶. When tumors
217 reached 2000 mm³, animals were sacrificed following institutional ethical guidelines. For
218 survival analysis, mice were censored at the time of sacrifice according to IACUC
219 guidelines. Tumors were rapidly extracted and formalin-fixed for immunohistochemical
220 analysis or stored at -80 °C for molecular analysis. Toxicity was monitored according to
221 weight loss three times per week. Weight loss greater than 15% was considered as a sign of
222 toxicity and these mice were sacrificed and excluded from the analysis.

223 **Statistical analysis**

224 Statistical analyses were performed using SPSS version 20 (SPSS Inc., IL, USA) or
225 GraphPad Prism software (San Diego, USA). $p < 0.05$ was considered significant. Values are
226 presented as mean \pm s.d. When data sets met normal distribution criteria, we used Student's
227 two-sided t-test analysis (for two-group comparisons) and one-way ANOVA analysis (if
228 more than two groups were compared). We used Bonferroni test as a post hoc test. If data
229 did not meet normal distribution criteria, we used Mann-Whitney test (for two-group
230 comparisons) and Kruskal-Wallis test (if more than two groups were compared). We used
231 Dunn's test as a post hoc test. *In vitro* experiments were repeated independently at least
232 three times, using technical triplicates. Variances were similar between groups in all
233 experiments, as determined by the F test using GraphPad Prism. For GSEA module
234 analysis, significance was corrected for multiple tests (FDR < 0.05). The sample size in each
235 *in vivo* experiment was based on our previous studies on such experiment^{13,19-21}. Mice that
236 were sacrificed due to treatment-related toxicity were excluded from the survival analyses.
237 The investigators were not blinded to allocation during experiments and analyses.

238 **Genomic profiling, Methylome profiling and data analysis**

239 See the Supplementary Materials and Methods section.

240 **Cell lines, plasmids and reagents, Decitabine demethylation treatment, *In vitro***
241 **functional cell assays, IGF2 immunostaining, Ligand mediated IGF pathway**
242 **activation, Reverse transcription (RT) Polymerase Chain Reaction (PCR) and**
243 **quantitative RT-PCR**

244 See the Supplementary Materials and Methods section.

245 **Metabolic toxicity in the HCC subcutaneous xenograft mouse model, Tumor**
246 **xenograft molecular characterization and *Igf2* and *HI9* expression analysis in mouse**
247 **models of HCC**

248 See the Supplementary Materials and Methods section.

249

250 **Results**

251 ***IGF2* overexpression in HCC is triggered by epigenetic mechanisms**

252 We and others have previously demonstrated that *IGF2* is overexpressed in human HCC
253 ^{13,14}. In this study, we conducted an integrative oncogenomic analysis of 228 human HCCs
254 to elucidate the underlying mechanism of *IGF2* enhanced expression. *IGF2* transcriptional
255 and protein levels were significantly higher compared with matched surrounding cirrhotic
256 and non-tumor liver tissues. *IGF2* was mainly expressed by hepatocytes, though bile duct
257 epithelial cells also expressed it to a lesser extent (**Figure 1A and Supplementary Figure**
258 **1**). *IGF2* overexpression above 20-fold was observed in 15% (34/228) of the samples,
259 among which 24 samples showed upregulation above 100-fold. Interestingly, the
260 expression of *INSR-A* isoform, a pro-proliferative receptor with high affinity for IGF2, was
261 upregulated in 38% (86/228) of HCCs, being significantly higher in *IGF2*-overexpressing
262 samples (**Supplementary Figure 2**). None of these events was significantly associated
263 with any clinic-pathological characteristics.

264 We previously reported that *IGF2* overexpression in HCC is associated with the
265 reactivation of its fetal promoters ¹³, but the mechanism responsible for this reactivation has
266 not been described yet. As *IGF2* is an imprinted gene, we hypothesized that epigenetic
267 deregulation could be the underlying cause. The methylation status of the *IGF2-H19*
268 imprinting control region (ICR1) and the *IGF2* promoters was evaluated in human HCCs
269 with low ($n = 173$; $FC < 20$) or high ($n = 27$; $FC \geq 20$) *IGF2* levels and in 10 healthy liver
270 samples. We observed hypomethylation in both alleles of the strongest fetal promoters (P3-
271 P4) and increased methylation of the adult promoter P1 in samples overexpressing *IGF2*

272 compared to low-*IGF2* and healthy liver samples (**Figure 1B and C, and Supplementary**
273 **Figure 3A-C**). This fetal promoter hypomethylation was associated with increased
274 expression of transcripts from P3, while increased methylation of P1 was associated with a
275 severe downregulation in P1-derived transcripts (**Supplementary Figure 3D and E**). *IGF2*
276 overexpression was also associated to hypomethylation of the *IGF2/H19* ICR1 and to
277 increased *H19* expression (**Figure 1C and Supplementary Figure 3A-C and F**).

278 We confirmed the association between aberrant methylation of *IGF2* promoters and *IGF2*
279 overexpression in human HCC cell lines. Hep3B and Huh7 presented the highest *IGF2*
280 levels when compared to normal liver, while SNU449 and PLC5 had the lowest expression
281 (**Supplementary Figure 4A**). Overexpression of the ligand was associated with higher
282 activation of the pathway (**Supplementary Figure 4B**). The methylation status of CpGs
283 located at fetal and adult promoters was evaluated in these cell lines (**Supplementary**
284 **Figure 4C and D**). HCC cells overexpressing *IGF2* displayed a decreased proportion of
285 methylated CpGs in P3-P4 compared to HCC cell lines with low *IGF2* levels. This aberrant
286 methylation was associated with an increased expression of transcripts derived from fetal
287 promoters and abrogated expression of those derived from the adult promoter
288 (**Supplementary Figure 4E**). As expected, forced demethylation of *IGF2* promoters by
289 decitabine treatment in SNU449 and PLC5 led to *IGF2* overexpression due to promoter
290 reactivation (**Supplementary Figure 5A**).

291 Furthermore, several microRNAs (miRNAs) have been shown to be involved in *IGF2*
292 deregulation: miR-483-5p, an intronic miRNA expressed from the *IGF2* locus, has been
293 reported to increase fetal *IGF2* mRNA levels ²³. Accordingly, patients in our cohort
294 overexpressing *IGF2* displayed significantly overexpression of miR-483-5p when

295 compared with low-*IGF2* HCCs (**Figure 1D**). A direct link between miR-483 and *IGF2*
296 expression was established *in vitro*. SNU449 and PLC5 *IGF2* expression levels were
297 significantly increased upon transfection of miR-483 (**Supplementary Figure 5B and C**).

298 Overexpression of *IGF2* from fetal promoters was detected in 94% (32/34) of our HCC
299 cohort, and out of these, 66% (21/32) of cases presented aberrant methylation of fetal
300 promoters while 53% (17/32) overexpress miR-483-5p, pointing to epigenetic mechanisms
301 as the main cause of re-expression of fetal *IGF2* in HCC (**Figure 1E and Supplementary**
302 **Figure 6**). Overall, these results suggest that DNA methylation deregulation is the
303 predominant cause of *IGF2* overexpression in human HCC samples, but alternative
304 epigenetic mechanisms, such as miRNA deregulation, could contribute to the reactivation
305 of fetal *IGF2*.

306 **IGF2 is an epi-driver in *in vivo* experimental models of HCC**

307 To evaluate the specific role of *IGF2* in HCC we established a genetically engineered
308 mosaic mouse model in which transposable elements containing *c-Myc/Akt1* and *Igf2* were
309 delivered into the liver of wild-type mice through hydrodynamic tail vein injection (**Figure**
310 **2A**)¹⁹⁻²¹. All *Igf2*-injected mice showed increased *IGF2* expression and constitutive
311 activation of the IGF pathway, as indicated by higher phosphorylation of IGF1R and its
312 downstream protein AKT (**Figure 2B and C**). Mice overexpressing *Igf2* presented
313 significant reduction of survival in comparison to control mice due to accelerated tumor
314 progression (**Figure 2D and E**). Importantly, all *Igf2*-overexpressing mice died 2.5 months
315 after plasmid delivery. Interestingly, liver-specific *Igf2* overexpression in knock-out mice
316 lacking the tumor suppressor p19^{Arf} did not promote tumor initiation (**Supplementary**

317 **Figure 7)**, suggesting that IGF2, although might not be a transforming oncogene *per se*,
318 significantly accelerates HCC progression.

319 Further evidence on the role of IGF2 in HCC tumorigenesis was obtained from the analysis
320 of *Igf2* expression of 11 HCC mouse models, including 10 available in GEO database and
321 one generated in our laboratory with CCl₄ and diethylnitrosamine (DEN)¹⁸. *Igf2* (FC>2)
322 was overexpressed in 10 models, with a prevalence ranging from 22-100% of the tumors.
323 Importantly, overexpression of *Igf2* was coupled to *H19* overexpression (FC>2) in all cases
324 **(Supplementary Table 6)**.

325

326 **IGF2 overexpression increases HCC proliferation**

327 To decipher the role of *IGF2* overexpression in enhancing hepatocarcinogenesis, the effect
328 of altered *IGF2* expression was evaluated *in vitro* through colony formation, apoptosis and
329 migration assays. *IGF2* knockdown using short hairpin RNAs was conducted in Hep3B and
330 Huh7 cells (*Hep3B-shIGF2*; *Huh7-shIGF2*), which present high endogenous *IGF2*
331 expression. On the other hand, *IGF2* ectopic overexpression was induced in SNU449 and
332 PLC5 cells (*SNU449-IGF2*; *PLC5-IGF2*), characterized by very low endogenous *IGF2*
333 levels **(Supplementary Figure 4A and B and Supplementary Figure 8A-C)**.
334 Downregulation of *IGF2* levels by >60% (shIGF2#2 and #3) caused a significant decrease
335 in colony number compared to controls **(Figure 3A, and Supplementary Figure 8D)**. On
336 the other hand, *SNU449-IGF2* and *PLC5-IGF2*, displayed a significant increase in the
337 number of colonies **(Figure 3B, and Supplementary Figure 8D)**. The colonies were also
338 bigger in size, indicating an increase in cell proliferation. However, the rate of cell death
339 and migration remained unaltered in both cases **(Supplementary Figure 9)**. Altogether,

340 these results provide evidence that IGF2-driven tumorigenesis in HCC relies on the
341 increase in cell proliferation rather than antiapoptotic or enhanced migratory effects.

342 **High *IGF2* levels correlate with an undifferentiated and aggressive phenotype**

343 To shed light on the functional consequences of *IGF2* overexpression in HCC, we carried
344 out Gene Set Enrichment Analysis (GSEA), Ingenuity Pathway Analysis (IPA) and
345 Comparative Marker Selection (CMS) using expression data from human HCC patients,
346 GEMM overexpressing IGF2 and HCC cell lines with ectopic overexpression or silencing-
347 mediated downregulation of IGF2. We found that expression profiles from HCC patients
348 with up-regulated *IGF2* were significantly associated with three equivalent molecular
349 subclasses of HCC ⁵: (a) the G1 molecular subclass ²⁴, which has been reported to
350 overexpress paternally imprinted genes such as *IGF2*; (b) the Proliferation subclass ²⁵,
351 characterized by IGF pathway activation; and (c) the S1-S2 proliferation subclasses ²⁶. In
352 addition, *IGF2*-overexpressing samples were associated with several hepatic progenitor
353 cell-like signatures ^{27,28}, hepatic stellate cell activation, NOTCH signaling ²⁹, genes up-
354 regulated in hepatoblastoma ³⁰, and tumor invasiveness ^{31,32}. We also observed enrichment
355 of poor-prognosis liver-cancer signatures ^{33,34} and up-regulation of VEGFA targets ^{35,36}
356 **(Figure 1E and Table 1)**. Furthermore, *IGF2* overexpression was associated with
357 significant upregulation of the hepatic progenitor-like markers *SALL4* ^{37,38} (mean FC 4.9 vs
358 1.4), *EPCAM* ²⁷ (mean FC 11.7 vs 1.4) and *KRT19* ²⁸ (mean FC 5.3 vs 0.8) and increased
359 alpha fetoprotein plasma levels (median 90 ng/dL vs 60 ng/dL) compared to low-*IGF2*
360 samples **(Supplementary Figure 10)**. GEMM tumors overexpressing IGF2 shared the
361 main characteristics of human IGF2-overexpressing tumors, particularly a more
362 proliferative, undifferentiated and invasive tumor profile **(Supplementary Table 7)**.

363 Consistently, target genes of IGF2 identified by comparing expression profiles of SNU449-
364 IGF2 and Hep3B-shIGF2 (**Supplementary Table 8**), were involved stem cell pluripotency,
365 cellular proliferation and survival (**Supplementary Table 9**). Taken together these data
366 suggest that the reexpression of fetal *IGF2* leads to HCCs with progenitor cell-like features
367 and aggressive phenotype.

368 **Antiproliferative effect of monoclonal antibodies against IGF ligands in human HCC** 369 **cell lines**

370 The marked overexpression of *IGF2* in HCC patients and the causal relationship between
371 IGF2 and accelerated tumor progression *in vivo* prompted us to assess the selective effect of
372 IGF2 blockage as a putative novel therapy for HCC. To this end, the effects of BI 836845, a
373 monoclonal antibody against IGF ligands (IGF1/2-mAb)¹⁶, were first evaluated *in vitro*
374 using HCC cell lines (**Supplementary Figure 3A and B**). A significant reduction in
375 colony number and colony size was observed in Hep3B and Huh7 cells when treated with
376 IGF1/2-mAb, but not in cells with low *IGF2* levels (**Figure 3C and D, and**
377 **Supplementary Figure 11A**). Consistently, the IGF1/2-mAb was able to significantly
378 reduce cell viability (>20%) in the two cell lines. BrdU incorporation showed that this
379 reduction was due to a decrease in the proliferation rate (**Supplementary Figure 11B, and**
380 **C**). In contrast, IGF1/2-mAb had no significant effect in cells with low *IGF2* levels
381 (**Supplementary Figure 11D and E**). No effects on apoptosis or migration were observed
382 (**Supplementary Figure 12A-C**). These results suggest that IGF1/2-mAb is capable of
383 attenuating IGF2-dependent cell proliferation *in vitro*. To confirm that the antiproliferative
384 effects of the antibody were specific for IGF2-blocking as opposed to IGF1, *shIGF2-* and
385 *IGF2-transfected* cell lines were subjected to colony formation assay after IGF1/2-mAb

386 treatment. In line with our preceding results, *Hep3B-shIGF2* and *Huh7-shIGF2*, contrary to
387 wild-type cells, were not sensitive to antibody treatment (**Figure 3A**). Moreover, forced
388 expression of *IGF2* in SNU449 and PLC5 cells promoted an increase in colony formation
389 that was abolished upon IGF1/2-mAb treatment (**Figure 3B**). Remarkably, IGF1/2-mAb
390 completely blocked IGF2-dependent activation of IGF1R and INSR in HCC cell lines,
391 while it had no effect on insulin-mediated pathway activation assessed by phosphorylation
392 of INSR (**Figure 3E, and Supplementary Figure 12D**). Conversely, IGF1R inhibition
393 with the TKI linsitinib simultaneously impaired both IGF2 and insulin-mediated pathway
394 activation. These results suggest that IGF1/2-mAb-based treatments, by simultaneously
395 blocking IGF2-dependent activation of IGF1R and INSR-A without affecting the metabolic
396 pathway, might be more efficient than other IGF1R-targeted therapies and better tolerated
397 than TKI-based therapies.

398 **IGF2 inhibition delays tumor growth and improves survival *in vivo***

399 The antioncogenic efficacy of IGF1/2-mAb was evaluated using an Hep3B xenografted
400 mouse model. Animals received vehicle, sorafenib (the standard of care), IGF1/2-mAb, or a
401 combination of both. Strikingly, tumor growth was significantly lower in the IGF1/2-mAb
402 and in the combination arm compared to either vehicle or sorafenib alone (**Figure 4A**).
403 These differences were more remarkable after 3 weeks, when tumor growth inhibition for
404 IGF1/2-mAb and the combination was maximum (**Figure 4B and C**). Furthermore, mice in
405 the IGF1/2-mAb- and combination arms exhibited significantly increased survival (**Figure**
406 **4D**) compared to both vehicle and sorafenib, respectively. Differences between single agent
407 IGF1/2-mAb and combined arms were not statistically significant at any time point.
408 Overall, all drugs were well tolerated, although three mice were sacrificed due to body

409 weight loss (one from the sorafenib arm (1/13) and two from the combination arm (2/13)).
410 No significant differences in blood glucose or glycosylated hemoglobin levels were
411 detected among arms further supporting the low toxicity related to this monoclonal
412 antibody (**Supplementary Figure 13 A-C**).

413 Molecular characterization of the xenografted HCC tumors confirmed the antiproliferative
414 effect of IGF1/2-mAb seen *in vitro* and unraveled an additional anti-angiogenic
415 mechanism. Specifically, significant reduction of Ki-67 staining was observed in all groups
416 compared to vehicle. IGF1/2-mAb and the combination presented stronger reduction in
417 proliferation than sorafenib (**Figure 5A**). Consistently, IGF1/2-mAb inhibited
418 phosphorylation of IGF1R and AKT, two well-known molecular players in proliferation
419 (**Figure 5B**). Additionally, staining for the endothelial marker CD31 showed that both
420 sorafenib and IGF1/2-mAb decreased tumor vascularization compared to vehicle (**Figure**
421 **5C**). No apoptotic events were detected (**Supplementary Figure 13D**). These results
422 indicate that the capacity of IGF1/2-mAb to impair tumor growth *in vivo* is not only due to
423 its strong antiproliferative effect, but also to inhibition of angiogenesis. Taken together,
424 IGF2 inhibition *in vivo* displays superior efficacy than sorafenib, the only approved
425 targeted therapy for HCC, emphasizing the relevance of IGF2 as a novel and efficient drug
426 target for HCC.

427 **Discussion**

428 The landscape of driver genes and epigenetic alterations in cancer has been thoroughly
429 reviewed⁹. Although epigenetic overexpression of different genes has been shown to be
430 sufficient to drive formation of cancer *in vivo* (e.g. bladder cancer³⁹), the biological
431 relevance of any candidate epi-driver has not yet been confirmed in HCC^{3,5-8}. Here we
432 present *IGF2*, which is re-expressed through epigenetic mechanisms, as the first actionable
433 validated epi-driver in HCC, and we propose monoclonal antibodies against this growth
434 factor as a potential targeted therapy in a defined subset of HCC patients.

435 We detected a high *IGF2* overexpression in 15% of HCC patients associated with aberrant
436 promoter methylation and miRNA deregulation. The fetal *IGF2*-promoter region was
437 heavily demethylated, while the adult promoter P1 was repressed^{40,41}, and thus this
438 aberrant methylation is proposed as the crucial mechanism leading to *IGF2* overexpression.
439 Our data suggest that the standard model of *IGF2* LOI does not apply to HCC (similarly to
440 other cancers⁴²⁻⁴⁴). LOI of *IGF2* is believed to occur through *IGF2/H19* ICR1
441 hypermethylation turning the monoallelic expression of *IGF2* into biallelic, and reducing
442 expression of *H19*⁴⁵. However, our data suggest that ICR1 is significantly hypomethylated
443 in most HCC samples and *H19* is overall upregulated. In fact, *IGF2* overexpression in liver
444 cancer cell lines is often associated to upregulation of *H19*^{46,47}. The coupled expression of
445 *Igf2* and *H19* that we observed in ten HCC mouse models suggests that these genes share
446 an aberrant epigenetic regulatory mechanism occurring during hepatocarcinogenesis.

447 Imprinted genes such as *IGF2* are overexpressed in somatic stem cells^{48,49}. We tested
448 whether tumors with high levels of *IGF2* were associated with self-renewal. We unravel a

449 significant association between *IGF2*-overexpressing HCCs and hepatic progenitor cell-like
450 signatures and progenitor markers (*SALL4*^{37,38}, *EPCAM*²⁷ and *KRT19*²⁸). Tumors with
451 progenitor cell-like origin are known to be more aggressive and undifferentiated²⁸, which
452 is consistent with the association of high-*IGF2* tumors with poor prognosis signatures. Our
453 experiments using mosaic GEMMs demonstrated that, although liver-specific *Igf2*
454 overexpression did not promote tumor initiation, when co-expressed with *Myc* and *Akt1*
455 oncogenes, it significantly enhanced HCC tumorigenesis and reduced survival. Further
456 analysis using HCC cells overexpressing or downregulating *IGF2* allowed us to define the
457 mechanism of action of IGF2-driven tumorigenesis, through increased proliferation.

458 The ability of this growth factor to accelerate tumor progression in a murine HCC model,
459 together with the overexpression of *IGF2* in 15% of HCC samples, suggests that direct
460 targeting of this ligand is an attractive therapeutic strategy for treatment of patients with
461 IGF2-dependent HCC tumors. BI 836845 (IGF1/2-mAb) is currently being tested in phase
462 I/II clinical trials in solid tumors (NCT02123823, NCT02204072). The mechanism of
463 action of IGF1/2-mAbs (BI 836845 or similar antibodies^{50,51}) is distinct from IGF1R-
464 targeted antibodies, which to date have shown discouraging results in clinical studies¹⁵.
465 Our results confirmed that BI 836845 offers the potential to inhibit IGF1R and INSR-A
466 activation without interfering with the insulin/INSR-B-dependent glucose metabolism. This
467 confers important advantages to previous attempts of blocking IGF signaling, since (a) the
468 expression of INSR-A variant is increased in HCC and represents a potential mechanism of
469 intrinsic resistance to IGF1R-targeted therapies⁵² and (b) the inhibition of insulin signaling
470 *in vivo* can result in severe metabolic toxic effects such as hyperglycemia and systemic
471 infections¹⁵.

472 BI 836845 blocked IGF2-mediated proliferation and displayed significant antitumor
473 activity. We expanded the preclinical evidence on this drug, which to date was restricted to
474 colon carcinoma and Ewing's sarcoma xenograft models ¹⁶. Unsurprisingly, the well-
475 known antiangiogenic effects of sorafenib ² were also observed with IGF1/2-mAb. IGF
476 signaling is involved in VEGFA production under hypoxic conditions. Hypoxia inducible
477 factors upregulate *IGF2* which in turn promotes *VEGFA* expression leading to angiogenesis
478 ^{53,54}. Moreover, it has been reported that blockage of *IGF2* expression causes
479 downregulation of *VEGFA* and inhibits growth in HCC cells ⁵⁵. This was further supported
480 by our GSEA and IPA analysis, where those samples with increased *IGF2* expression
481 presented strong association with VEGF activation. Altogether, these results suggest that
482 IGF2 might play a role in regulating tumor angiogenesis in HCC, consistent with the
483 reduced vascularization observed in the xenograft model. Since tumor cells secreting IGF2
484 are able to circumvent the antiangiogenic effects of IGF1R-targeted antibodies by signaling
485 through the INSR-A ⁵⁶, the antioncogenic effects of IGF1/2-mAbs are in part due to its
486 ability to neutralize IGF2/IGF1R/INSR-A-mediated angiogenic activity ^{51,57}.

487 Intriguingly, no synergic effects were found in mice treated with a combination of IGF1/2-
488 mAb and sorafenib, suggesting a high dependency of Hep3B tumors on IGF2. This
489 suggests that the subset of HCC patients overexpressing *IGF2* may benefit from a precision
490 medicine approach using IGF1/2-mAbs. One of the limitations of the current study is that
491 we proposed a cut-off to define overexpression of IGF2 levels (>20 fold), but we do not
492 have enough information on what is the ideal biomarker to be tested in early clinical trials.
493 Thus, whether the biomarker for enrichment of HCC-subset is based upon transcriptional

494 expression of IGF2 or based on other means, such as immunohistochemistry, needs to be
495 further explored.

496 After sorafenib approval, all molecular targeted therapies failed to provide survival
497 advantages ⁴. In order to overcome this problem, more effective drugs targeting all comers
498 should be tested in clinical trials. Alternatively, proof of concept trials ³ based on
499 biomarkers able to recognize HCC subpopulations might be critical for precision medicine.
500 Herein, we propose a new concept to be explored and tested in the clinical setting capable
501 to benefit a subgroup of patients overexpressing the epi-driver IGF2.

502 **References**

- 503 1. Anon. Global, regional, and national age–sex specific all-cause and cause-specific
504 mortality for 240 causes of death, 1990–2013: a systematic analysis for the Global
505 Burden of Disease Study 2013. *Lancet* 2014;385:117–71.
- 506 2. Llovet JM, Ricci S, Mazzaferro V, et al. Sorafenib in advanced hepatocellular
507 carcinoma. *N. Engl. J. Med.* 2008;359:378–90.
- 508 3. Llovet JM, Villanueva A, Lachenmayer A, et al. Advances in targeted therapies for
509 hepatocellular carcinoma in the genomic era. *Nat. Rev. Clin. Oncol.* 2015;12:408-
510 24.
- 511 4. Llovet JM, Hernandez-Gea V. Hepatocellular Carcinoma: Reasons for Phase III
512 Failure and Novel Perspectives on Trial Design. *Clin. Cancer Res.* 2014;20:2072–9.
- 513 5. Zucman-Rossi J, Villanueva A, Nault J-C, et al. Genetic Landscape and Biomarkers
514 of Hepatocellular Carcinoma. *Gastroenterology* 2015;149:1226–1239.e4.
- 515 6. **Schulze K, Imbeaud S, Letouzé E**, et al. Exome sequencing of hepatocellular
516 carcinomas identifies new mutational signatures and potential therapeutic targets.
517 *Nat. Genet.* 2015;47:505–11.
- 518 7. **Villanueva A, Portela A**, Sayols S, et al. DNA Methylation-based prognosis and
519 epidrivers in hepatocellular carcinoma. *Hepatology* 2015;61:1945-56.
- 520 8. **Totoki Y, Tatsuno K, Covington KR**, et al. Trans-ancestry mutational landscape
521 of hepatocellular carcinoma genomes. *Nat. Genet.* 2014;46:1–10.
- 522 9. Vogelstein B, Papadopoulos N, Velculescu VE, et al. Cancer genome landscapes.
523 *Science* 2013;339:1546–58.

- 524 10. Feng H, Yu Z, Tian Y, et al. A CCRK-EZH2 epigenetic circuitry drives
525 hepatocarcinogenesis and associates with tumor recurrence and poor survival of
526 patients. *J. Hepatol.* 2015;62:1100–11.
- 527 11. Northcott PA, Pfister SM, Jones DTW. Next-generation (epi)genetic drivers of
528 childhood brain tumours and the outlook for targeted therapies. *Lancet. Oncol.*
529 2015;16:e293–302.
- 530 12. Kim TK, Gore SD, Zeidan AM. Epigenetic Therapy in Acute Myeloid Leukemia:
531 Current and Future Directions. *Semin. Hematol.* 2015;52:172–83.
- 532 13. Tovar V, Alsinet C, Villanueva A, et al. IGF activation in a molecular subclass of
533 hepatocellular carcinoma and pre-clinical efficacy of IGF-1R blockage. *J Hepatol*
534 2010;52:550–559.
- 535 14. Breuhahn K, Longerich T, Schirmacher P. Dysregulation of growth factor signaling
536 in human hepatocellular carcinoma. *Oncogene* 2006;25:3787–800.
- 537 15. Pollak M. The insulin and insulin-like growth factor receptor family in neoplasia: an
538 update. *Nat. Rev. Cancer* 2012;12:159–169.
- 539 16. Friedbichler K, Hofmann MH, Kroeze M, et al. Pharmacodynamic and
540 Antineoplastic Activity of BI 836845, a Fully Human IGF Ligand-Neutralizing
541 Antibody, and Mechanistic Rationale for Combination with Rapamycin. *Mol.*
542 *Cancer Ther.* 2014;13:399–409.
- 543 17. Vu TH, Hoffman AR. Promoter-specific imprinting of the human insulin-like
544 growth factor-II gene. *Nature* 1994;371:714–7.
- 545 18. **Dapito DH, Mencin A, Gwak G-Y, Pradere JP**, et al. Promotion of hepatocellular
546 carcinoma by the intestinal microbiota and TLR4. *Cancer Cell* 2012;21:504–16.

- 547 19. **Kang T-W, Yevsa T, Woller N, et al.** Senescence surveillance of pre-malignant
548 hepatocytes limits liver cancer development. *Nature* 2011;479:547–551.
- 549 20. Wuestefeld T, Pesic M, Rudalska R, Dauch D, et al. A Direct in vivo RNAi screen
550 identifies MKK4 as a key regulator of liver regeneration. *Cell* 2013;153:389–401.
- 551 21. **Rudalska R, Dauch D, Longerich T, et al.** In vivo RNAi screening identifies a
552 mechanism of sorafenib resistance in liver cancer. *Nat. Med.* 2014;20:1138–46.
- 553 22. Tang TC, Man S, Lee CR, et al. Impact of metronomic UFT/cyclophosphamide
554 chemotherapy and antiangiogenic drug assessed in a new preclinical model of
555 locally advanced orthotopic hepatocellular carcinoma. *Neoplasia* 2010;12:264–74.
- 556 23. Li X, Nadauld L, Ootani A, et al. Oncogenic transformation of diverse
557 gastrointestinal tissues in primary organoid culture. *Nat. Med.* 2014;20:769–77.
- 558 24. Boyault S, Rickman DS, Reyniès A de, et al. Transcriptome classification of HCC is
559 related to gene alterations and to new therapeutic targets. *Hepatology* 2007;45:42–
560 52.
- 561 25. Chiang DY, Villanueva A, Hoshida Y, et al. Focal gains of VEGFA and molecular
562 classification of hepatocellular carcinoma. *Cancer Res.* 2008;68:6779–88.
- 563 26. Hoshida Y, Nijman SMB, Kobayashi M, et al. Integrative transcriptome analysis
564 reveals common molecular subclasses of human hepatocellular carcinoma. *Cancer*
565 *Res.* 2009;69:7385–92.
- 566 27. Yamashita T, Forgues M, Wang W, et al. EpCAM and α -Fetoprotein Expression
567 Defines Novel Prognostic Subtypes of Hepatocellular Carcinoma. *Cancer Res.*
568 2008;68:1451–61.

- 569 28. Villanueva A, Hoshida Y, Battiston C, et al. Combining clinical, pathology, and
570 gene expression data to predict recurrence of hepatocellular carcinoma.
571 *Gastroenterology* 2011;140:1501–12.e2.
- 572 29. **Villanueva A, Alsinet C**, Yanger K, et al. Notch signaling is activated in human
573 hepatocellular carcinoma and induces tumor formation in mice. *Gastroenterology*
574 2012;143:1660–69.e7.
- 575 30. **Cairo S, Armengol C**, Reyniès A De, et al. Hepatic stem-like phenotype and
576 interplay of Wnt/beta-catenin and Myc signaling in aggressive childhood liver
577 cancer. *Cancer Cell* 2008;14:471–84.
- 578 31. Anastassiou D, Rumjantseva V, Cheng W, Huang J, Canoll P, Yamashiro D and
579 Kandel J. Human cancer cells express Slug-based epithelial-mesenchymal transition
580 gene expression signature obtained in vivo. *BMC Cancer* 2011;11:529.
- 581 32. **Gotzmann J, Fischer ANM, Zojer M**, et al. A crucial function of PDGF in TGF- β -
582 mediated cancer progression of hepatocytes. *Oncogene* 2006;25:3170–85.
- 583 33. Woo HG, Park ES, Cheon JH, et al. Gene expression-based recurrence prediction of
584 hepatitis B virus-related human hepatocellular carcinoma. *Clin Cancer Res*
585 2008;14:2056–64.
- 586 34. Lee J-SS, Chu I-SS, Heo J, et al. Classification and prediction of survival in
587 hepatocellular carcinoma by gene expression profiling. *Hepatology* 2004;40:667–
588 76.
- 589 35. Weston GC, Haviv I, Rogers PAW. Microarray analysis of VEGF-responsive genes
590 in myometrial endothelial cells. *Mol. Hum. Reprod.* 2002;8:855–63.

- 591 36. Schoenfeld J, Lessan K, Johnson N, et al. Bioinformatic analysis of primary
592 endothelial cell gene array data illustrated by the analysis of transcriptome changes
593 in endothelial cells exposed to VEGF-A and PlGF. *Angiogenesis* 2004;7:143–56.
- 594 37. Yong KJ, Gao C, Lim JSJ, et al. Oncofetal gene SALL4 in aggressive hepatocellular
595 carcinoma. *N. Engl. J. Med.* 2013;368:2266–76.
- 596 38. Oikawa T, Kamiya A, Zeniya M, Chikada H, Hyuck AD, Yamazaki Y, Wauthier E,
597 Tajiri H, Miller LD, Wang XW, Reid LM, Nakauchi H. Sal-like protein 4
598 (SALL4), a stem cell biomarker in liver cancers. *Hepatology* 2013;57:1469–83.
- 599 39. Palmboos PL, Wang L, Yang H, et al. ATDC/TRIM29 drives invasive bladder cancer
600 formation through microRNA-mediated and epigenetic mechanisms. *Cancer Res.*
601 2015 ;75 :5155-66.
- 602 40. Li X, Nong Z, Ekström C, et al. Disrupted IGF2 promoter control by silencing of
603 promoter P1 in human hepatocellular carcinoma. *Cancer Res.* 1997;57:2048–54.
- 604 41. **Tang S, Hu W, Hu J**, et al. Hepatitis B virus X protein promotes P3 transcript
605 expression of the insulin-like growth factor 2 gene via inducing hypomethylation of
606 P3 promoter in hepatocellular carcinoma. *Liver Int.* 2015;35:608–19.
- 607 42. Cheng Y-W, Idrees K, Shattock R, et al. Loss of imprinting and marked gene
608 elevation are 2 forms of aberrant IGF2 expression in colorectal cancer. *Int. J.*
609 *Cancer* 2010;127:568–77.
- 610 43. Murphy SK, Huang Z, Wen Y, et al. Frequent IGF2/H19 domain epigenetic
611 alterations and elevated IGF2 expression in epithelial ovarian cancer. *Mol. Cancer*
612 *Res.* 2006;4:283–92.

- 613 44. Kondo M, Suzuki H, Ueda R, et al. Frequent loss of imprinting of the H19 gene is
614 often associated with its overexpression in human lung cancers. *Oncogene*
615 1995;10:1193–8.
- 616 45. Robertson KD. DNA methylation and human disease. *Nat. Rev. Genet.* 2005;6:597–
617 610.
- 618 46. Kim KS, Lee YI. Biallelic expression of the H19 and IGF2 genes in hepatocellular
619 carcinoma. *Cancer Lett.* 1997;119:143–8.
- 620 47. Li X, Adam G, Cui H, et al. Expression, promoter usage and parental imprinting
621 status of insulin-like growth factor II (IGF2) in human hepatoblastoma: uncoupling
622 of IGF2 and H19 imprinting. *Oncogene* 1995;11:221–9.
- 623 48. Berg JS, Lin KK, Sonnet C, et al. Imprinted genes that regulate early mammalian
624 growth are coexpressed in somatic stem cells. *PLoS One* 2011;6:e26410.
- 625 49. Venkatraman A, He XC, Thorvaldsen JL, et al. Maternal imprinting at the H19-Igf2
626 locus maintains adult haematopoietic stem cell quiescence. *Nature* 2013;500:345–9.
- 627 50. Gao J, Chesebrough JW, Cartlidge SA, et al. Dual IGF-I/II-Neutralizing Antibody
628 MEDI-573 Potently Inhibits IGF Signaling and Tumor Growth. *Cancer Res.*
629 2011;71:1029–40.
- 630 51. Dransfield DT, Cohen EH, Chang Q, et al. A human monoclonal antibody against
631 insulin-like growth factor-II blocks the growth of human hepatocellular carcinoma
632 cell lines in vitro and in vivo. *Mol. Cancer Ther.* 2010;9:1809–19.
- 633 52. Livingstone C. IGF2 and cancer. *Endocr. Relat. Cancer* 2013;20:R321–39.
- 634 53. Bae SK, Bae MH, Ahn MY, et al. Egr-1 mediates transcriptional activation of IGF-
635 II gene in response to hypoxia. *Cancer Res.* 1999;59:5989–94.

- 636 54. Kim KW, Bae SK, Lee OH, et al. Insulin-like growth factor II induced by hypoxia
637 may contribute to angiogenesis of human hepatocellular carcinoma. *Cancer Res.*
638 1998;58:348–51.
- 639 55. **Yao N, Yao D, Wang L**, et al. Inhibition of autocrine IGF-II on effect of human
640 HepG2 cell proliferation and angiogenesis factor expression. *Tumor Biol.*
641 2012;33:1767–76.
- 642 56. **Bid HK, Zhan J**, Phelps DA, et al. Potent inhibition of angiogenesis by the IGF-1
643 receptor-targeting antibody SCH717454 is reversed by IGF-2. *Mol. Cancer Ther.*
644 2012;11:649–59.
- 645 57. Bid HK, London CA, Gao J, et al. Dual targeting of the type 1 insulin-like growth
646 factor receptor and its ligands as an effective antiangiogenic strategy. *Clin. Cancer*
647 *Res.* 2013;19:2984–94.

648 Author names in bold designate shared co-first authors.

649

650 **Acknowledgments**

651 We thank Judit Peix, Monica Higuera and Laia Cabellos for technical assistance and Juan
652 José Lozano for bioinformatic support. Boehringer Ingelheim supplied the monoclonal
653 antibody BI 836845 used in this study.

654 **Figure Legends**

655 **Figure 1. *IGF2* overexpression in HCC is driven by epigenetic mechanisms. (A)** *IGF2*
656 levels determined by quantitative RT-PCR in healthy liver samples ($n = 10$), adjacent non-
657 tumor (NT) tissue ($n = 47$) and HCC tumors ($n = 228$). Dots represent the expression value
658 of each individual sample and the line is the mean value of each group. Overexpression of
659 *IGF2* was defined as >20-fold. Statistical significance between groups is calculated by
660 Kruskal-Wallis with Dunn's multiple comparison test. **(B)** Schematic representation of the
661 methylation pattern in *IGF2* adult promoter (blue) and fetal promoters (green). **(C)**
662 Methylation levels measured by methylome array in CpGs of the maternal allele located
663 within adult promoter (P1), fetal promoters (P3-P4) and the *IGF2/H19* imprinting locus
664 (ICR1) in 200 HCC samples expressing low (blue; $n = 173$) or high (red; $n = 27$) *IGF2*
665 levels. Dots represent the mean value in each CpG and bars the SD between samples. Fold
666 change is normalized to 1 (mean expression value in healthy liver). **(D)** Expression analysis
667 of miR-483-5p in HCC patients with low (blue; $n = 190$) or high (red; $n = 28$) *IGF2* levels.
668 Error bars are mean \pm SD. Statistical significance between groups is calculated by two-
669 sided t-test. **(E)** Schematic representation of epigenetic deregulations affecting each of the
670 34 *IGF2*-overexpressing tumors in our cohort and its integration with the current molecular
671 classification of HCC²⁴⁻²⁶. Statistical significance is calculated by χ^2 test.

672 **Figure 2. *IGF2* contributes to HCC progression in a transposon-based mouse model.**

673 **(A)** Schematic representation of transposable elements encoding *Myc/Akt1* and *Igf2*. Caggs,
674 CAGGS promoter; IR/DR, inverted repeats and direct repeats; IRES, internal ribosome
675 entry site. **(B)** *Igf2* expression levels measured by qRT-PCR in tumors of mice upon
676 intrahepatic delivery of *Myc/Akt1*- and either an *Igf2* expressing transposon ($n = 7$) or a

677 transposon without any gene (Control) ($n = 6$). Fold change is normalized to 1 (mean
678 expression value in healthy livers of control mice). Dots represent the expression value of
679 each individual sample and the line is the mean value of each group. Statistical significance
680 between groups is calculated by Mann-Whitney test. * $p < 0.05$, ** $p < 0.01$, *** $p < 0.001$. (C)
681 Western blot analysis of murine livers upon delivery of corresponding constructs
682 (representative pictures; $n = 4$). Intrahepatic delivery of *Igf2* induces overexpression of
683 IGF2 and the consequent phosphorylation (activation) of IGF1R and its downstream target
684 AKT. (D) Survival analysis (Kaplan-Meier) of mice upon intrahepatic delivery of *Myc/Akt1*
685 and either an *Igf2* expressing transposon ($n = 7$) or a transposon without gene expression
686 (Control) ($n = 6$). For survival analysis, mice were censored at the time of sacrifice
687 according to IACUC guidelines. Statistical significance was calculated using a log-rank
688 test. (E) Representative images and H&E (20x magnification) staining of mice livers upon
689 intrahepatic delivery of *Myc/Akt1* and either an *Igf2* expressing transposon or a transposon
690 without a gene (Control).

691 **Figure 3. IGF2 blockage by shIGF2 and IGF1/2-mAb on HCC cell lines impairs cell**
692 **proliferation.** (A) Quantification of colony formation assay using Hep3B or Huh7 cell
693 lines stably transfected with shMock or shIGF2#2, and treated with the IGF1/2-mAb. Error
694 bars are mean \pm SD. corresponding to ≥ 3 experiments in triplicate. Statistical significance
695 between groups is calculated by one-way ANOVA with post hoc Bonferroni test in all
696 panels. * $p < 0.05$, ** $p < 0.01$, *** $p < 0.001$ (vs. non-treated sh-Mock) or # $p < 0.05$, ## $p < 0.001$,
697 #### $p < 0.0001$ (vs. shMock treated with IGF1/2-mAb). (B) Quantification of colony
698 formation assay using SNU449 or PLC5 cell lines stably transfected a Control vector or an
699 IGF2-overexpression vector, and treated with the IGF1/2-mAb. * $p < 0.05$, ** $p < 0.01$,

700 *** $p < 0.001$ (vs. non-treated Control) or # $p < 0.05$, ## $p < 0.001$, ### $p < 0.0001$ (vs. Control
701 treated with IGF1/2-mAb). (C) Quantification of colony formation assay using Hep3B or
702 Huh7 cell lines treated with different concentrations of IGF1/2-mAb. (D) Quantification of
703 colony formation assay using SNU449 or PLC5 cell lines treated with different
704 concentrations of IGF1/2-mAb. * $p < 0.05$, ** $p < 0.01$, *** $p < 0.001$ (vs Non-treated). (E)
705 Representative Western Blot analysis of Hep3B (high *IGF2*) cell lysates stimulated by
706 IGF2 or Insulin and treated with IGF1R TKI or IGF1/2-mAb for 15 min. Tubulin was used
707 as a loading control.

708 **Figure 4. IGF1/2-mAb and its combination with sorafenib delay tumor growth and**
709 **improve survival in subcutaneous xenografted HCC tumors.** (A) Tumor growth in mice
710 treated with sorafenib ($n = 13$), IGF1/2-mAb ($n = 12$), a combination of sorafenib and
711 IGF1/2-mAb ($n = 13$) or vehicle ($n = 8$). Error bars are mean \pm SD. Statistical significance
712 between groups is calculated by one-way ANOVA with post hoc Bonferroni test. (B)
713 Representative picture of tumors in each group after 21 days of treatment. (C) Percentage
714 of tumor growth inhibition (TGI) of sorafenib ($n = 13$), IGF1/2-mAb ($n = 12$) and
715 combination ($n = 13$) compared to vehicle ($n = 8$) after 7, 14 or 21 days of treatment.
716 Statistical significance between sorafenib and other treatment groups is calculated by one-
717 way ANOVA with post hoc Bonferroni test. * $p < 0.05$, ** $p < 0.01$, *** $p < 0.001$. (D) Survival
718 analysis (Kaplan-Meier) of mice upon treatment with sorafenib ($n = 13$), IGF1/2-mAb ($n =$
719 12), a combination of sorafenib and IGF1/2-mAb ($n = 13$) or vehicle ($n = 8$). Statistical
720 significance between groups is calculated by log-rank test.

721 **Figure 5. IGF1/2-mAb delays tumor growth by inhibiting proliferation and**
722 **angiogenesis.** (A) *Left*: Quantification of Ki-67 positive stained nuclei in 10 fields (40x

723 magnification). Bars are mean \pm SD. ($n = 5$ mice/group). Statistical significance between
724 vehicle and treated groups is calculated by one-way ANOVA with post hoc Bonferroni test.
725 * $p < 0.05$, ** $p < 0.01$, *** $p < 0.001$. *Right*: Representative pictures of Ki-67 staining. **(B)** *Left*:
726 Quantification of the percentage of CD31⁺ area stained in 10 fields (20x magnification)
727 relative to vehicle. Bars are mean \pm SD. ($n = 5$ mice/group). Statistical significance
728 between vehicle and treated groups is calculated by one-way ANOVA with post hoc
729 Bonferroni test. * $p < 0.05$, ** $p < 0.01$, *** $p < 0.001$. *Right*: Representative pictures of CD31
730 staining. **(C)** Representative Western Blot analysis of tumor lysates from vehicle- ($n = 3$),
731 sorafenib- ($n = 3$), IGF1/2-mAb- ($n = 3$), and combination-treated mice ($n = 3$). Tubulin
732 was used as a loading control.

Table 1. Human HCCs displaying high *IGF2* levels are portrayed by an hepatic progenitor cell-like and aggressive phenotype. Association of gene signatures was evaluated using the GSEA Module from GenePattern. NES denotes Normalized Enrichment Score in gene-set enrichment analysis. A NES score higher than 1 indicates enrichment of the gene-set in high-IGF2 HCC. FDR, false discovery rate. The Broad Institute Gene Set enrichment analysis website (www.broad.mit.edu/gsea) provides detailed information about the computational method. Association of signaling pathways was evaluated using Ingenuity Pathway Analysis (www.ingenuity.com).

Gene signatures associated to IGF2 overexpression in HCC (GSEA)					Signaling pathways associated to IGF2 overexpression in HCC (IPA)	
	Gene signature	p value	FDR	NES	Signaling pathway	p value
Hepatic progenitor cell-like	VILLANUEVA_LIVER_CANCER_CK19 ²⁸	<0.0001	<0.0001	2.314	Human Embryonic Stem Cell Pluripotency	0.04
	YAMASHITA_LIVER_CANCER_WITH_EPCAM_UP ²⁷	<0.0001	0.005	1.857	Hepatic Stellate Cell Activation	0.02
	REACTOME_ACTIVATED_NOTCH1_SIGNAL_TO_THE_NUCLEUS	<0.0001	0.009	1.958	Notch signaling	0.03
	PID_NOTCH_PATHWAY	0.002	0.01	1.919		
	REACTOME_SIGNALING_BY_NOTCH1	0.002	0.03	1.788		
	KEGG_NOTCH_SIGNALING_PATHWAY	<0.0001	0.03	1.788		
	REACTOME_SIGNALING_BY_NOTCH	<0.0001	0.04	1.734		
VILLANUEVA_NOTCH_SIGNALING ²⁹	<0.0001	0.01	1.811			
Hepatoblastoma	CAIRO_HEPATOBLASTOMA_UP ³⁰	<0.0001	0.01	1.672		
Poor prognosis	LEE_LIVER_CANCER_SURVIVAL_DN ³⁴	<0.0001	0.006	2.016		
	WOO_LIVER_CANCER_RECURRENCE_UP ³³	<0.0001	<0.0001	2.786		
Proliferation	BOYAULT_LIVER_CANCER_SUBCLASS_G1_UP ²⁴	<0.0001	<0.0001	3.201	Molecular mechanisms of cancer	0.01
	CHIANG_LIVER_CANCER_SUBCLASS_PROLIFERATION_UP ²⁵	<0.0001	<0.0001	2.751		
	HOSHIDA_LIVER_CANCER_SUBCLASS_S1 ²⁶	<0.0001	0.004	2.058		
	HOSHIDA_LIVER_CANCER_SUBCLASS_S2 ²⁶	<0.0001	0.004	2.056		
Invasiveness	ANASTASSIOU_CANCER_MESENCHYMAL_TRANSITION ³¹	<0.0001	0.000	2.316	Epithelial Adherens Junction Signaling	0.03
	GOTZMANN_EPITHELIAL_TO_MESENCHYMAL_TRANSITION_UP ³²	<0.0001	0.004	2.056		
Angiogenesis	WESTON_VEGFA_TARGETS ³⁵	<0.0001	0.03	1.771	VEGF Signaling	0.03
	VEGF_A_UP.V1_UP ^{<sup>36</sup>}	<0.0001	0.02	1.635		

Figure 1

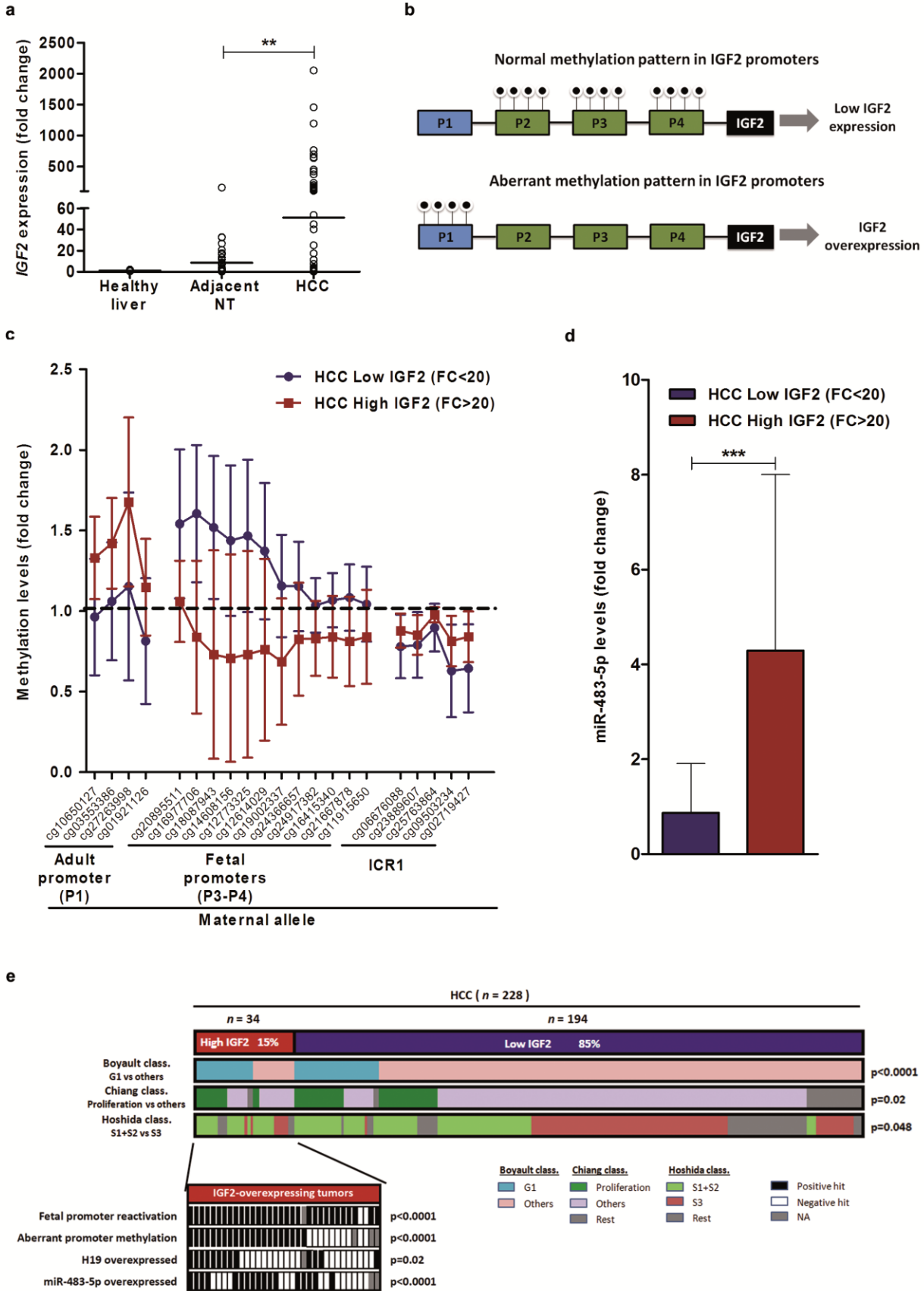


Figure 2

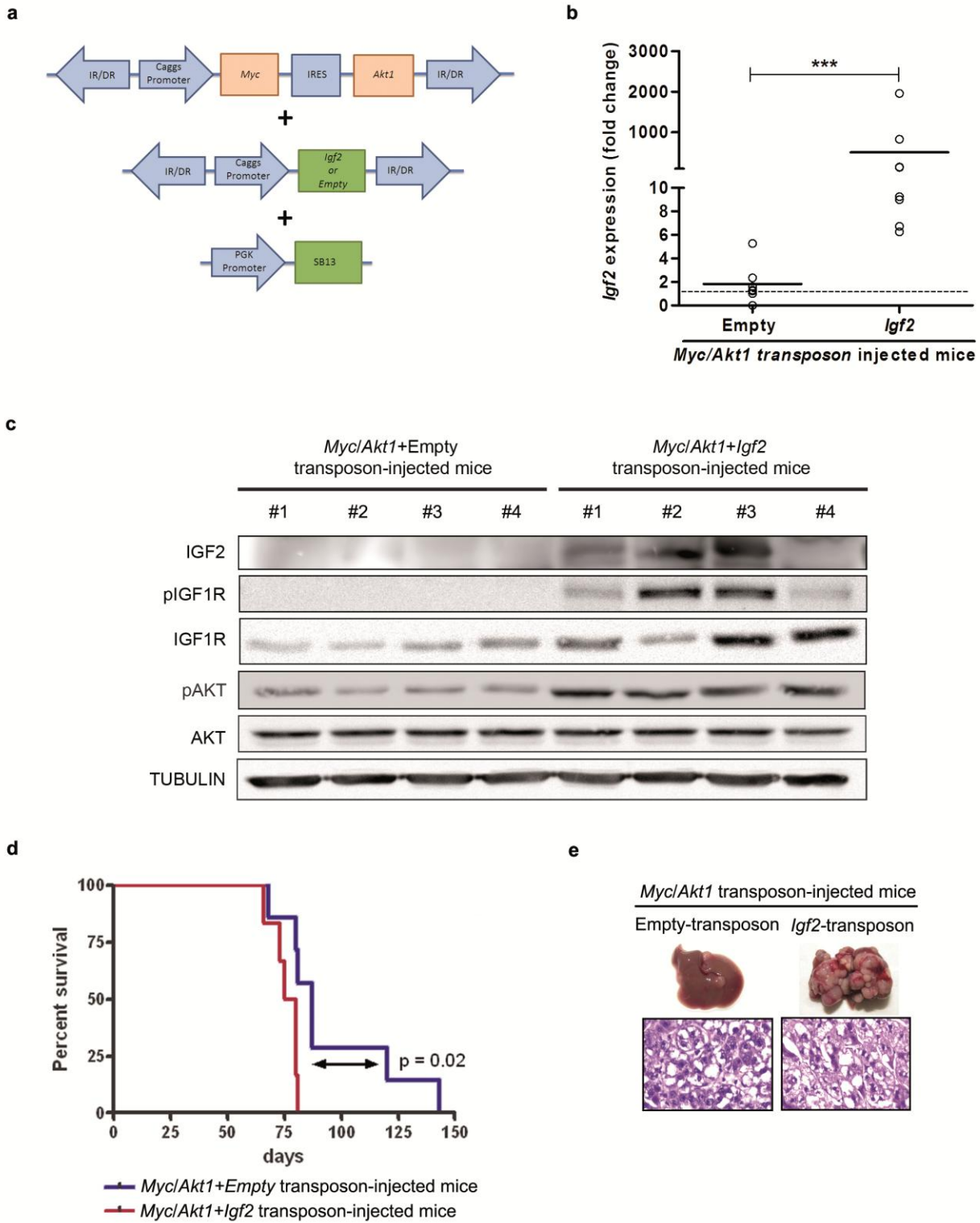


Figure 3

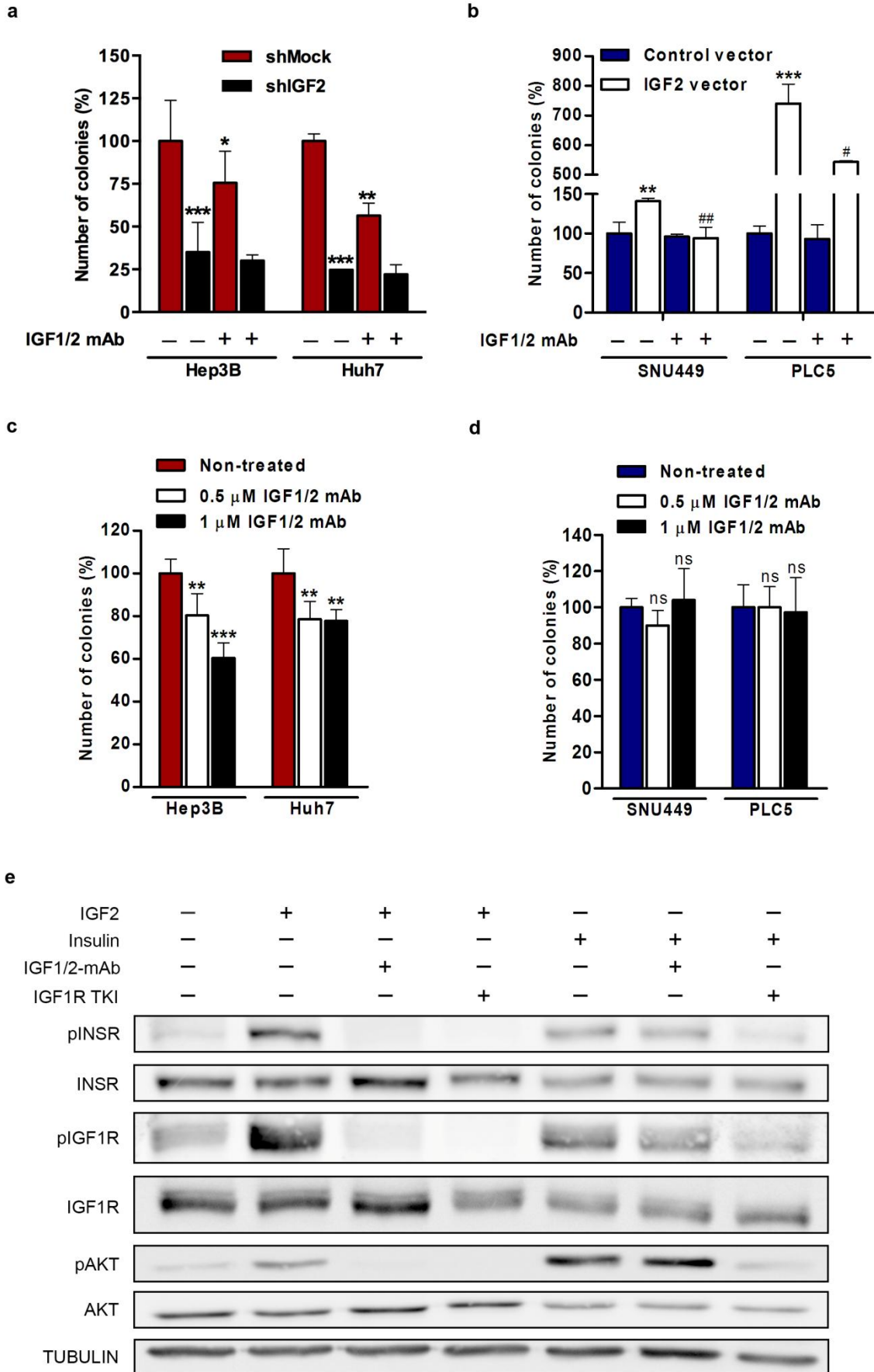


Figure 4

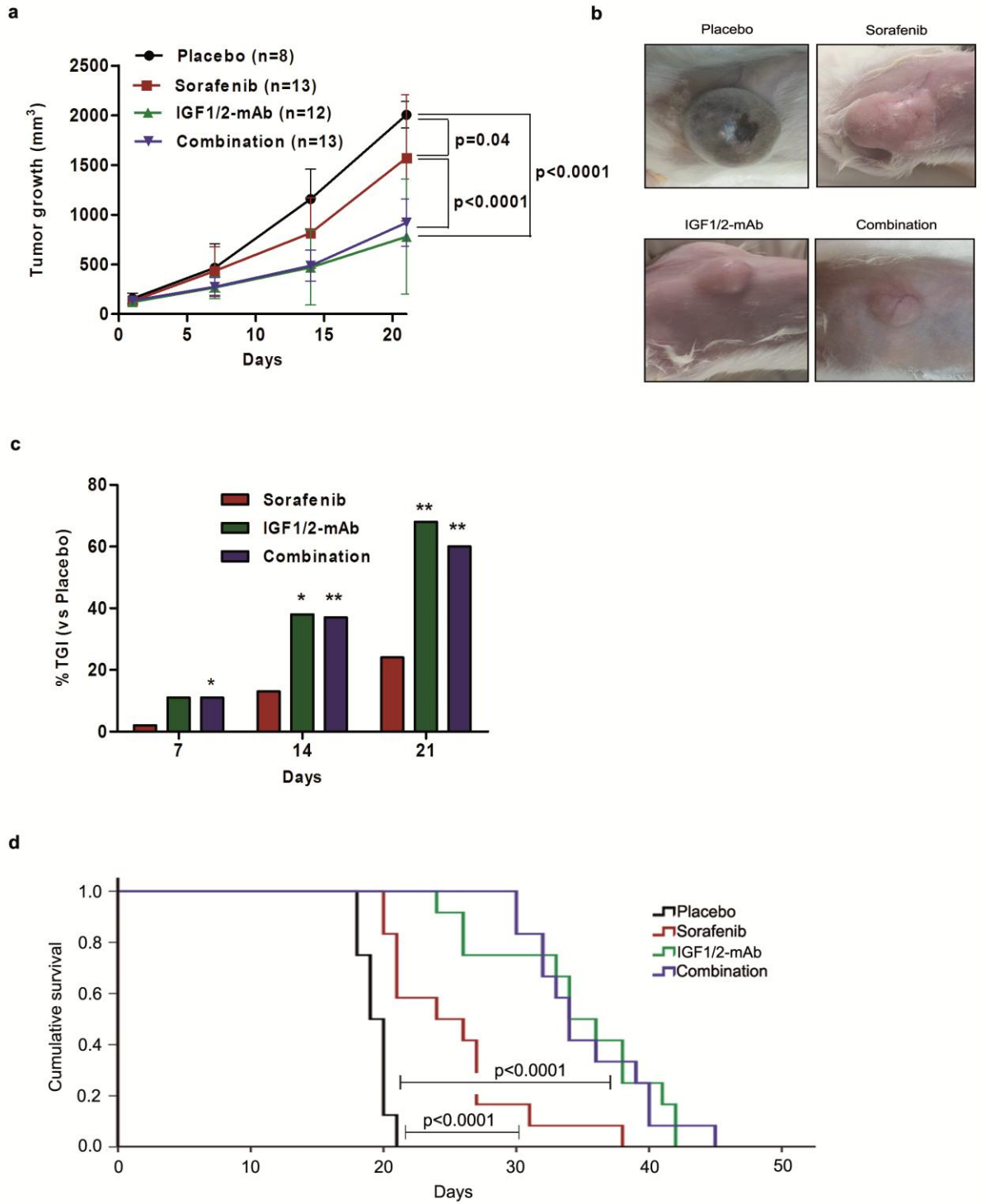
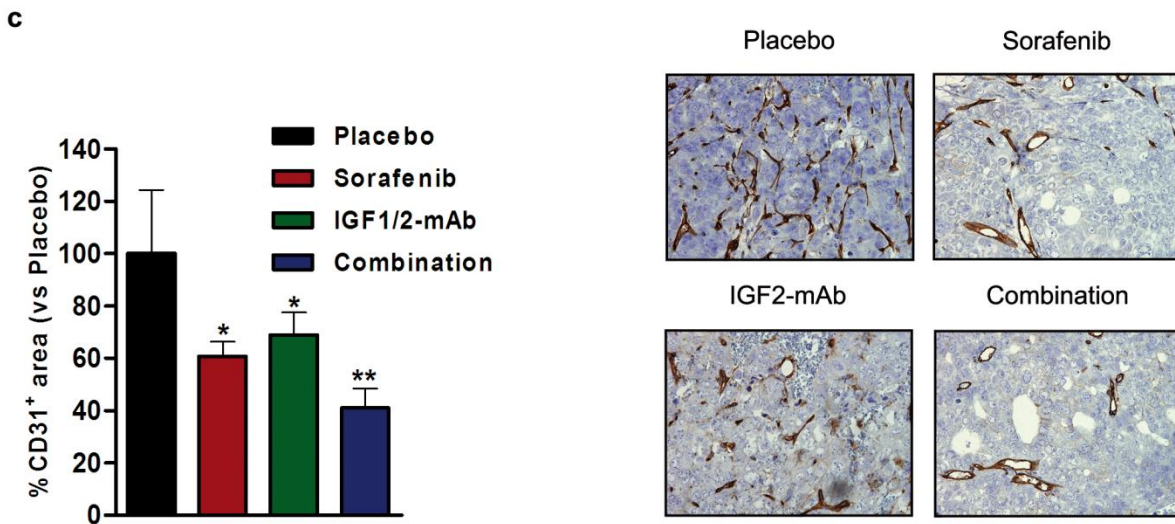
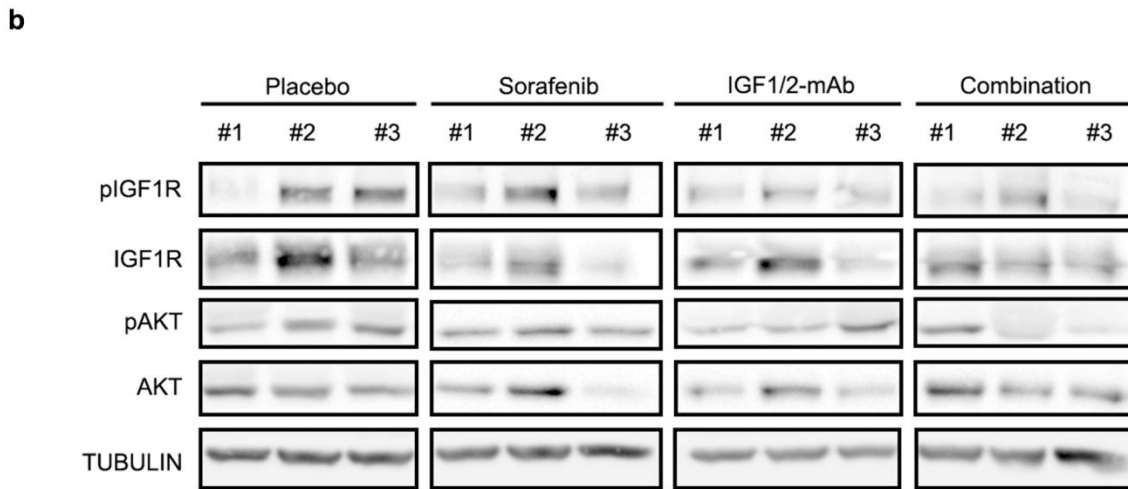
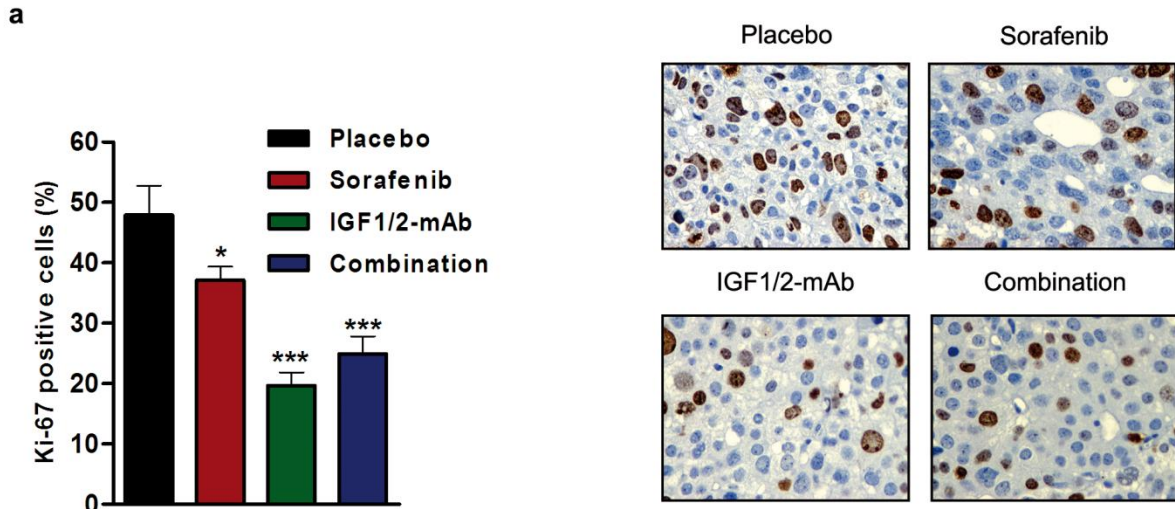


Figure 5



Supplementary Index

- **Supplementary Table 1.** Clinical characteristics of HCC patients..... p.39
- **Supplementary Table 2.** Methylation probes located at *IGF2* promoters and *IGF2-H19* ICR1..... p.40
- **Supplementary Table 3.** Primers for bisulfite conversion sequencing..... p.41
- **Supplementary Table 4.** Target sequences of shIGF2..... p.41
- **Supplementary Table 5.** List of Taqman probes used for quantitative RT-PCR..... p.41
- **Supplementary Table 6.** *Igf2* and *H19* expression in mouse models of HCC..... p.42
- **Supplementary Table 7.** HCCs from mouse injected with *Myc+Akt+Igf2* reproduce the genetic features of human tumors overexpressing *IGF2*..... p.43
- **Supplementary Table 8.** List of genes potentially regulated by *IGF2* in HCC cell lines..... p.44
- **Supplementary Table 9.** Top Canonical Pathways regulated by *IGF2*..... p.45
- **Supplementary Figure 1.** *IGF2* immunostaining in HCC human tumors..... p.46-47
- **Supplementary Figure 2.** Overexpression of *INSR-A* in HCC..... p.47
- **Supplementary Figure 3.** Aberrant methylation pattern in *IGF2* promoters is associated with *IGF2* overexpression in human HCC samples..... p.48-50
- **Supplementary Figure 4.** Aberrant methylation pattern in *IGF2* promoters is associated with *IGF2* overexpression in HCC cell lines..... p.51-52
- **Supplementary Figure 5.** Demethylation of *IGF2* fetal promoters leads to their reactivation and *IGF2* overexpression in HCC cell lines..... p.53-54
- **Supplementary Figure 6.** Epigenetic deregulations affecting the 228 tumors in our cohort..... p.54
- **Supplementary Figure 7.** *Igf2* overexpression alone is not able to initiate hepatocarcinogenesis in *in vivo* models..... p.55-56
- **Supplementary Figure 8.** Effects of *IGF2* on HCC cell proliferation..... p.57-58
- **Supplementary Figure 9.** *IGF2* has no effect in cell death and migration of HCC cells..... p.59-60
- **Supplementary Figure 10.** Upregulation of hepatic progenitor cell markers and increased plasma AFP levels are associated with *IGF2* re-expression in HCC..... p.61-62
- **Supplementary Figure 11.** Anti-proliferative effects of *IGF1/2*-mAb in HCC cell lines overexpressing *IGF2*..... p.63-64
- **Supplementary Figure 12.** *IGF1/2*-mAb has no effects in cell death and migration of HCC cells..... p.65-66
- **Supplementary Figure 13.** *IGF1/2*-mAb and its combination with sorafenib are well tolerated in HCC xenograft model..... p.67
- **Supplementary Materials and Methods**..... p.68-74

Supplementary Table 1. Clinical characteristics of HCC patients

Variable	Cohort (n=228)
Median age	66
Gender (male)	180 (79%)
Etiology	
Hepatitis C	103 (45%)
Hepatitis B	48 (21%)
Alcohol	33 (14%)
Others	38 (17%)
Child-Pugh score:	
A	222 (97%)
B	3 (1%)
Tumour size (cm)	
<2	28 (12%)
2-3	72 (32%)
>3	126 (55%)
Multiple nodules	
No	169 (74%)
Yes	57 (25%)
Micro-vascular invasion	
No	146 (64%)
Yes	67 (29%)
Satellites	
No	164 (72%)
Yes	63 (28%)
BCLC early stage (0-A)	197 (86%)
Degree of tumour differentiation	
Well	33 (14%)
Moderately	107 (47%)
Poor	44 (19%)
Bilirubin (≥ 1 mg/dL)	94 (41%)
Albumin (<3.5 g/L)	24 (11%)
Platelet count (<100,000/mm ³)	43 (19%)
AFP (>100 mg/dL)	53 (23%)
Events	
Recurrence	154 (66%)
Death	133 (58%)

Supplementary Table 2. Methylation probes located at *IGF2* promoters and *IGF2-H19* ICR1

Target	Probe ID
<i>IGF2</i> P1 promoter_maternal allele	cg10650127
<i>IGF2</i> P1 promoter_maternal allele	cg03553386
<i>IGF2</i> P1 promoter_maternal allele	cg27263998
<i>IGF2</i> P1 promoter_maternal allele	cg01921126
<i>IGF2</i> P1 promoter_paternal allele	cg08686462
<i>IGF2</i> P1 promoter_paternal allele	cg27331871
<i>IGF2</i> P1 promoter_paternal allele	cg25742037
<i>IGF2</i> P3-P4_maternal allele	cg20895511
<i>IGF2</i> P3-P4_maternal allele	cg16977706
<i>IGF2</i> P3-P4_maternal allele	cg18087943
<i>IGF2</i> P3-P4_maternal allele	cg14608156
<i>IGF2</i> P3-P4_maternal allele	cg12773325
<i>IGF2</i> P3-P4_maternal allele	cg12614029
<i>IGF2</i> P3-P4_maternal allele	cg19002337
<i>IGF2</i> P3-P4_maternal allele	cg24366657
<i>IGF2</i> P3-P4_maternal allele	cg24917382
<i>IGF2</i> P3-P4_maternal allele	cg16415340
<i>IGF2</i> P3-P4_maternal allele	cg21667878
<i>IGF2</i> P3-P4_maternal allele	cg11915650
<i>IGF2</i> P3-P4_paternal allele	cg20766090
<i>IGF2</i> P3-P4_paternal allele	cg02166532
<i>IGF2</i> P3-P4_paternal allele	cg08162473
<i>IGF2</i> P3-P4_paternal allele	cg03760951
<i>IGF2</i> P3-P4_maternal allele	cg20339650
<i>IGF2-H19</i> ICR1_maternal allele	cg06676088
<i>IGF2-H19</i> ICR1_maternal allele	cg25763864
<i>IGF2-H19</i> ICR1_maternal allele	cg09503234
<i>IGF2-H19</i> ICR1_maternal allele	cg23889607
<i>IGF2-H19</i> ICR1_maternal allele	cg02719427
<i>IGF2-H19</i> ICR1_paternal allele	cg26913576
<i>IGF2-H19</i> ICR1_paternal allele	cg00221747
<i>IGF2-H19</i> ICR1_paternal allele	cg02045936

Supplementary Table 3. Primers for bisulfite conversion sequencing

Primer	Sequence 5' → 3'
FW_Meth_P1	gctagcttggggaagaggtt
RV_Meth_P1	ctaggaggtgggggctatgt
FW_Meth_P3	ccgcctcctctcatctacc
RV_Meth_P3	gaaggttgcgggagaaaga

Supplementary Table 4. Target sequences of shIGF2

Name	Target sequence
shIGF2#1	ccacaaaagctcagaaattgg
shIGF2#2	ggccattcggaacattggaca
shIGF2#3	tcctggagacgtactgtgcta
Mock shRNA	gcttcgcgccgtagtctta

Supplementary Table 5. List of Taqman probes used for quantitative RT-PCR

Target Gene	Taqman Assay ID or Sequence (Reference)
Human <i>IGF2</i>	Hs01005963_m1
Human <i>IGF2</i> P1-derived	Hs01005962_m1
Human <i>IGF2</i> P3-derived	Hs00171254_m1
Human <i>INSR-A</i>	5'-TCCCCAGGCCATCT-3' ²⁶
Human <i>18S</i>	Hs99999901_s1
Human <i>H19</i>	Hs00262142_g1
Mouse <i>Igf2</i>	Mm00580426_g1
Mouse <i>H19</i>	Mm01156721_g1
Mouse <i>Rn18s</i>	Mm03928990_g1
Human miR-23b	002126
Human miR-483-5p	002338

Supplementary Table 6. *Igf2* and *H19* expression in mouse models of HCC. *Igf2* and *H19* mRNA levels were assessed by qRT-PCR in the chemically (DEN+CCl₄) induced mouse model and by microarray in 10 other mouse models of HCC with expression datasets available in GEO database (<http://www.ncbi.nlm.nih.gov/geo/>). FC was normalized to 1 using the mean expression value of the mouse healthy liver. A FC>2 was considered overexpression. Statistical significance between groups is calculated by Mann-Whitney test.

Mouse model	GEO DataSet	% of tumors overexpressing <i>Igf2</i> (FC>2)	Mean <i>Igf2</i> FC (vs healthy liver)	p-value	% of tumors overexpressing <i>H19</i> (FC>2)	Mean <i>H19</i> FC (vs healthy liver)	p-value
Chemically induced by DEN+CCl₄	Unpublished data	30% (3/10)	106.9	ns	80% (8/10)	84.0	ns
Notch constitutive activation	GSE33486	80% (4/5)	26.8	0.02	80% (4/5)	43.5	0.02
<i>Txnip</i> KO	GSE2127	78% (7/9)	6.0	0.03	100% (9/9)	40.1	0.006
<i>Pdgf-c</i> transgenic	GSE31431	60% (3/5)	2.3	0.02	60% (3/5)	2.3	ns
HBsAg induced HCC	GSE15251	100% (2/2)	110.8	0.02	NA	NA	NA
HBsAg + Aflatoxin B induced HCC	GSE54054	22% (2/9)	3.2	0.02	78% (7/9)	20.8	0.0006
Chemically induced by B6C3F1	GSE26538	67% (4/6)	42.3	ns	100% (6/6)	242.5	0.002
Triple KO (RB, p130, p107)	GSE19004	80 % (4/5)	123.7	ns	100% (5/5)	587.6	0.02
<i>Mdr2</i>-KO + Partial hepatectomy	GSE61422	33% (2/6)	3.8	ns	50% (3/6)	3.0	ns
WHV/<i>c-myc</i> transgenic	GSE39401	NA (mix of five tumors)	104.5	NA	NA (mix of five tumors)	601.5	NA
<i>Iqgap2</i> KO	GSE46646	0% (0/3)	0.4	ns	0% (0/3)	0.5	0.02

Supplementary Table 7. HCCs from mouse injected with *Myc+Akt+Igf2* reproduce the genetic features of human tumors overexpressing IGF2. Association of gene signatures was evaluated using the GSEA Module from GenePattern. Association of signaling pathways was evaluated using Ingenuity Pathway Analysis (www.ingenuity.com)

	Gene signatures associated to IGF2 overexpression in HCC (GSEA)				Signaling pathways associated to IGF2 overexpression in HCC (IPA)		
	Gene signature	p value	FDR	NES	Signaling pathway	p value	
Hepatic progenitor cell-like/ Undifferentiated cancer	VILLANUEVA_LIVER_CANCER_CK19 ²⁹	<0.0001	<0.0001	2.439	Embryonic Development	<0.0001	
	YAMASHITA_LIVER_CANCER_WITH_EPCAM_UP ²⁸	<0.0001	<0.0001	2.332			
	RHODES_UNDIFFERENTIATED_CANCER	<0.0001	<0.0001	2.539			
	ZHANG_BREAST_CANCER_PROGENITORS_UP	<0.0001	<0.0001	2.288			
	BHATTACHARYA_EMBRYONIC_STEM_CELL	<0.0001	<0.0001	2.258			
Hepatoblastoma/ Embryonic liver	CAIRO_LIVER_DEVELOPMENT_UP ³¹	0.002	0.04	1.590			
	CAIRO_HEPATOBLASTOMA_UP ³¹	<0.0001	0.02	1.663			
Poor prognosis	LEE_LIVER_CANCER_SURVIVAL_DN ³⁵	<0.0001	<0.0001	2.762			
Proliferation	BOYALT_LIVER_CANCER_SUBCLASS_G123_UP ²⁵	<0.0001	0.005	1.809	Cellular growth and proliferation	<0.0001	
	CHIANG_LIVER_CANCER_SUBCLASS_PROLIFERATION_UP ²⁶	<0.0001	<0.0001	2.580			
	HOSHIDA_LIVER_CANCER_SUBCLASS_S1 ²⁷	<0.0001	0.001	1.914			
		HOSHIDA_LIVER_CANCER_SUBCLASS_S2 ²⁷	0.002	0.02	1.696	Cell cycle	<0.0001
		REACTOME_DNA_REPLICATION	<0.0001	<0.0001	2.708		
		REACTOME_CELL_CYCLE_MITOTIC	<0.0001	<0.0001	2.655		
	REACTOME_CELL_CYCLE_CHECKPOINTS	<0.0001	<0.0001	2.322			
Invasiveness	SARRIO_EPITHELIAL_MESENCHYMAL_TRANSITION_UP	<0.0001	<0.0001	2.552			
	GOTZMANN_EPITHELIAL_TO_MESENCHYMAL_TRANSITION_UP ³³	<0.0001	0.007	1.782			
	JECHLINGER_EPITHELIAL_TO_MESENCHYMAL_TRANSITION_UP	0.005	0.03	1.614			
	ALONSO_METASTASIS_EMT_UP	<0.0001	0.003	1.855			
	KAPOSI_LIVER_CANCER_MET_UP	0.02	0.02	1.687			
	ROESSLER_LIVER_CANCER_METASTASIS_UP	<0.0001	0.03	1.631			
	WANG_TUMOR_INVASIVENESS_UP	<0.0001	<0.0001	2.205			
Angiogenesis	ABE_VEGFA_TARGETS_2HR	<0.0001	<0.05	1.549			

Supplementary Table 8. List of genes potentially regulated by IGF2 in HCC cell lines. Comparative Marker Selection Module from GenePattern was applied to compare the genetic profile of Hep3B-shIGF2 vs Hep3B-shMock and SNU449-IGF2 vs SNU449-Control. Only genes with FDR<0.05, FC>2 and common to both conditions were selected.

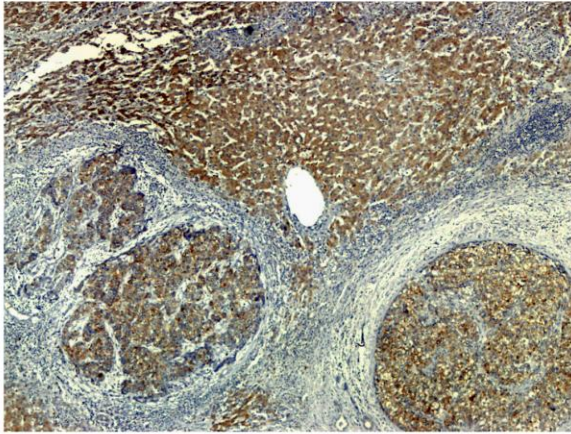
ANPEP	MIS18A	ACP2	FEZ2	PBX3
TAF9B	PAPSS1	ARHGEF38	CDCA5	ADAM15
NUP54	CDK10	FAM46B	CDCA7	ARL6IP1
NUP107	EXOG	SMCO4	USP7	FYTTD1
PRKAG2	MED20	RAE1	EED	PGLYRP4
CENPN	QSOX1	NDUFAF3	C7orf49	LIG3
SDC1	TDG	FGD5	GLG1	FAU
DBNL	DENR	RFC3	TMEM14A	MMAB
SART3	DZIP3	XXYL1	CDCA4	TBCD
RPN2	NFKBIA	MRPL49	HACD3	MOV10
ESRP2	MCM2	RFC5	SNRPF	NKX3-1
PDIA4	PLAUR	TPMT	ARMC5	HS3ST1
LYSMD1	TTC3P1	PTPN1	PACSIN3	ZNF572
CMTM6	ATXN7L2	KDEL1	SGK2	FADD
ABCF1	IFI30	BATF	ALDH18A1	CXXC4
LSM6	GID8	C6orf89	COL5A2	TLDC1
GALNT2	FUOM	CCNE1	PSRC1	GRHL1
EFEMP1	CYP2R1	OS9	UBE2D3	EXOSC9
TOR1AIP1	CREG1	ARL2BP	EZH2	PIGS
NOP56	ZNF764	NAP1L3	RNF146	PRMT3
ALDH1A3	BACE2	PIK3CD	POGK	CASP3
STK26	WDR77	ANTXR2	MPDU1	MPHOSPH9
TROAP	PRCP	OAZ2	MSL2	PDSS2
SLC44A1	GINS1	PLEKHG6	ARF5	APIP
THOC6	SIX4	TMEM132E	COX19	DGKZ
CFLAR	E2F7	SOAT1	SENP1	MEST
ANXA10	RBM15B	CDYL	TCAIM	USP13
PSMD2	DOLK	SCAMP3	MYBL2	LARS2
OTUD7B	SCAF4	ARHGEF26	S100A16	CAPRIN2
SPATA2	RNMTL1	CPXM2	FTSJ2	SCPEP1
NFYA	C2CD5	FLII	NME4	POU3F3
CPM	HLA-F	TRA2B	FAM133A	CDK4
SFXN2	TACC3	PPP1R1A	FAM111B	GLYCTK
UNG	SSR2	RNF219	GLIPR1	LHFP
SLC38A3	ARMC8	CENPW	SRRT	TMEM256
CXCL1	EXT2	PRELP	CANT1	VTA1
MPP5	TAF10	SGK1	PCOLCE2	RIC8A

Supplementary Table 9. Top Canonical Pathways regulated by IGF2

Canonical Pathway	p-value
Mammalian embryonic stem cell pluripotency	1.37E-03
Cellular growth and proliferation	2.16E-03
Cell death and survival	2.21E-03
IGF-1 Signaling	6.09E-04

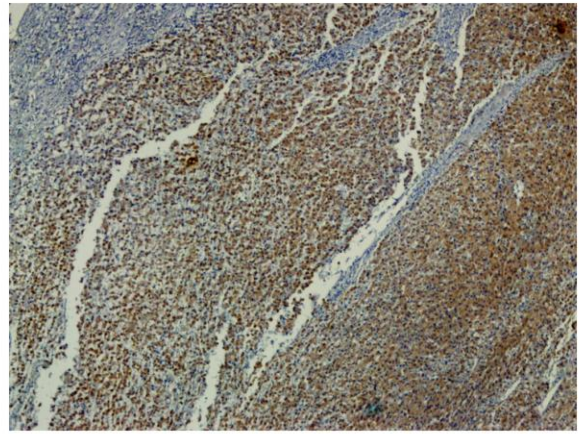
A

HCC

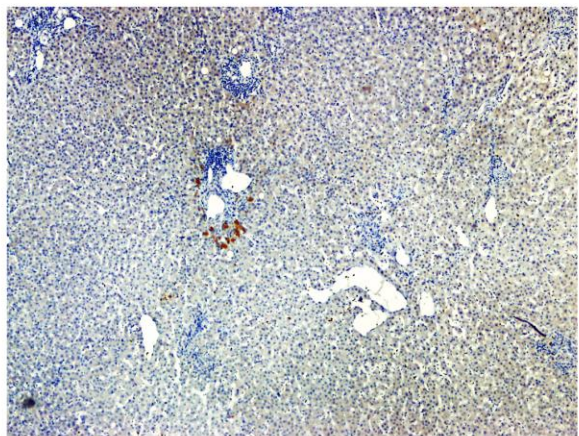
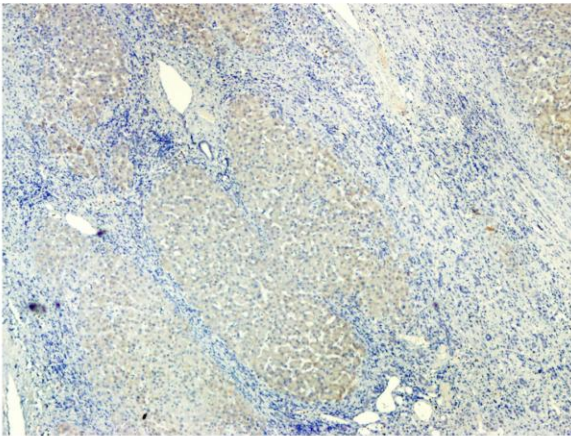


Cirrhotic adjacent tissue

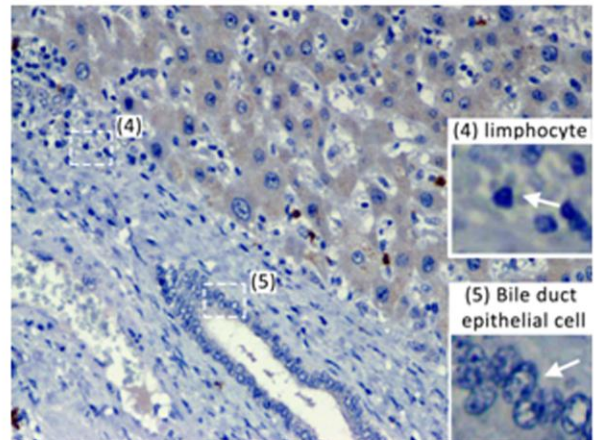
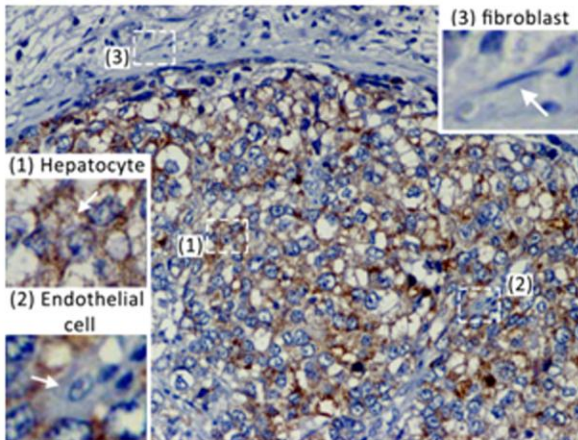
HCC



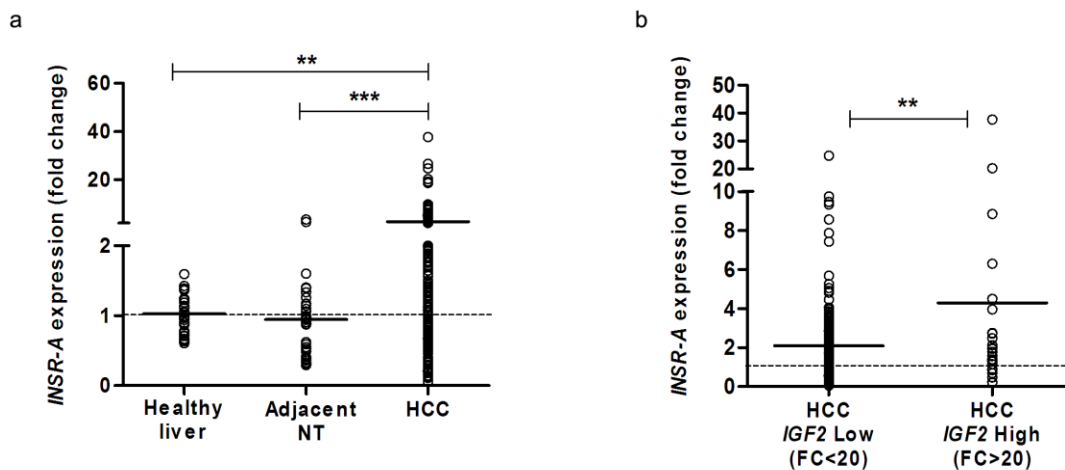
Non-cirrhotic adjacent tissue



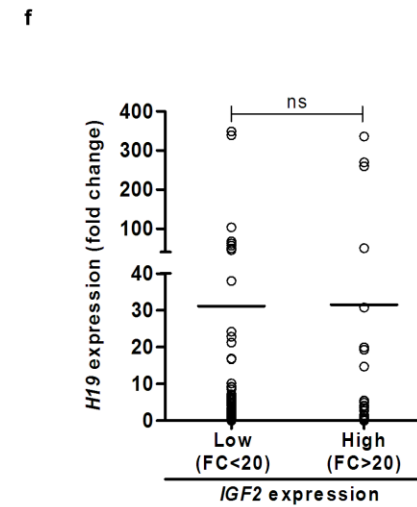
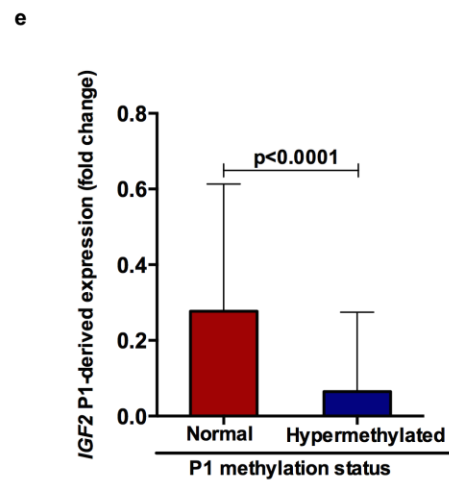
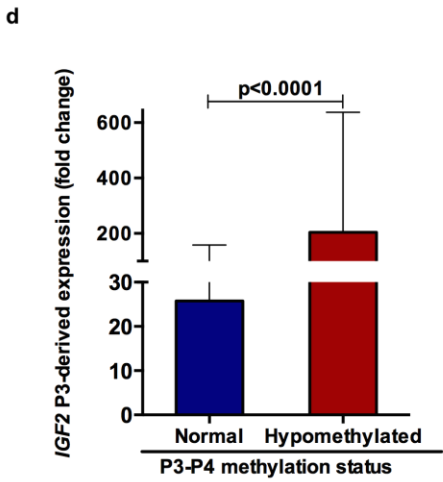
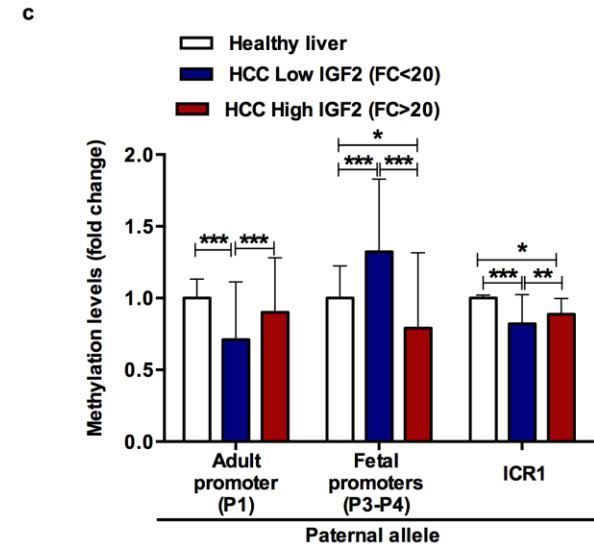
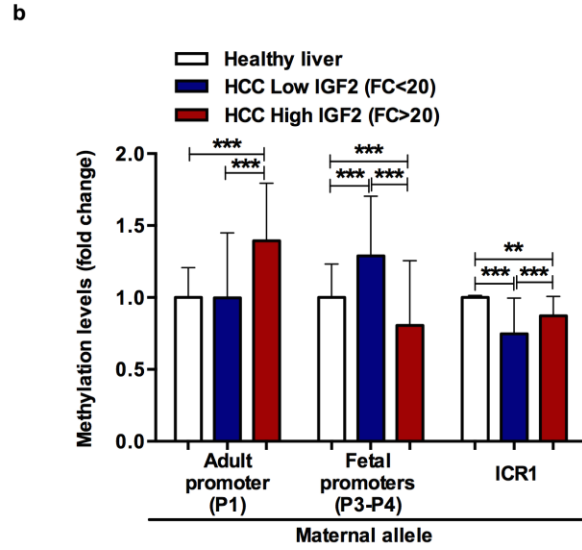
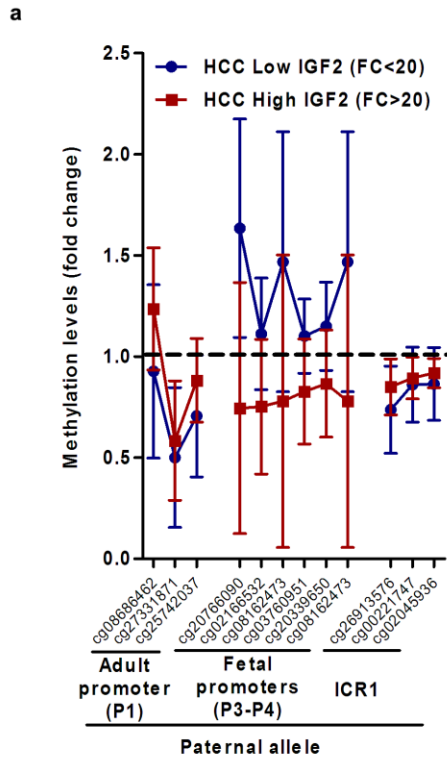
B



Supplementary Figure 1. IGF2 immunostaining in HCC human tumors. (A) Representative images of IGF2 protein levels in tumor and adjacent cirrhotic and non-cirrhotic tissue. (B) Cell types producing IGF2 in HCC tumors.

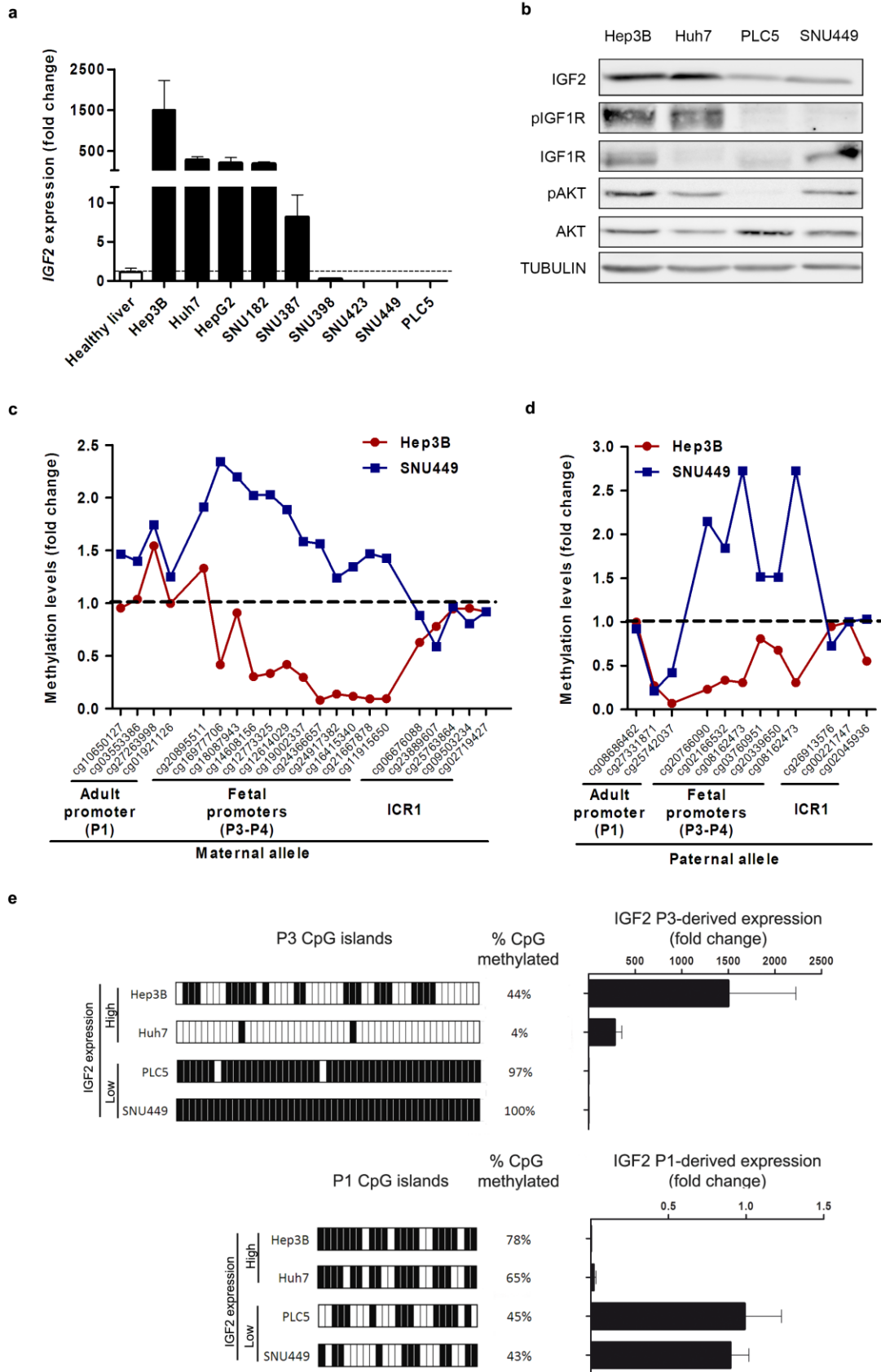


Supplementary Figure 2. Overexpression of *INSR-A* in HCC. (A) *INSR-A* isoform levels determined by quantitative RT-PCR in healthy liver samples ($n = 10$), adjacent non-tumor (NT) tissue ($n = 47$) and HCC tumors ($n = 228$). Dots represent the expression value of each individual sample and the line is the mean value of each group. Fold change is normalized to 1 (mean expression value in healthy liver). Overexpression of *INSR-A* was defined as >2-fold. Statistical significance between groups is calculated by Kruskal-Wallis with Dunn's multiple comparison test. * $p < 0.05$, ** $p < 0.01$, *** $p < 0.001$. (B) *INSR-A* isoform levels determined by quantitative RT-PCR in HCC samples with low ($n = 194$) or high ($n = 34$) *IGF2* expression. Dots represent the expression value of each individual sample and the line is the mean value of each group. Fold change is normalized to 1 (mean expression value in healthy liver). Statistical significance between groups is calculated by Mann-Whitney test. * $p < 0.05$, ** $p < 0.01$, *** $p < 0.001$.

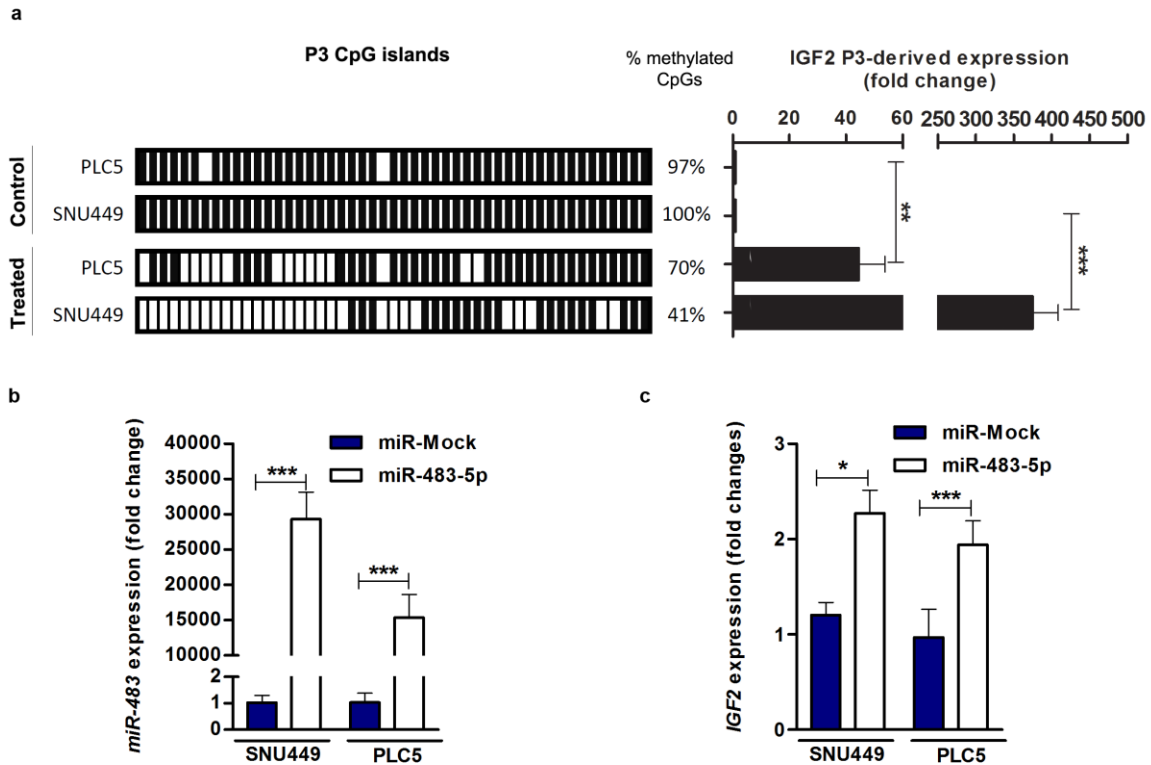


Supplementary Figure 3. Aberrant methylation pattern in *IGF2* promoters is associated with *IGF2* overexpression in human HCC samples. (A) Methylation levels measured by methylome array in CpGs of the paternal allele located within adult promoter (P1), fetal promoters (P3-P4) and the *IGF2/H19* imprinting locus (ICR1) in 200 HCC samples expressing low (blue; $n = 173$) or high (red; $n = 27$) *IGF2* levels. Dots represent the mean value in each CpG and bars the SD. between samples. Fold change is normalized to 1 (mean expression value in healthy liver). (B) Methylation levels measured by methylome array in CpGs located within adult promoter (P1), fetal promoters (P3-P4) and the *IGF2/H19* imprinting locus (ICR1) of the maternal allele in 10 healthy liver samples and 200 HCC samples expressing low ($n = 173$) or high ($n = 27$) *IGF2* levels. Fold change is normalized to 1 (mean expression value in healthy liver). Statistical significance between groups is calculated by Kruskal-Wallis with Dunn's multiple comparison test. * $p < 0.05$, ** $p < 0.01$, *** $p < 0.001$. (C) Methylation levels measured by methylome array in CpGs located within adult promoter (P1), fetal promoters (P3-P4) and the *IGF2/H19* imprinting locus (ICR1) of the paternal allele in 10 healthy liver samples and 200 HCC samples expressing low ($n = 173$) or high ($n = 27$) *IGF2* levels. Fold change is normalized to 1 (mean expression value in healthy liver). Statistical significance between groups is calculated by Kruskal-Wallis with Dunn's multiple comparison test. * $p < 0.05$, ** $p < 0.01$, *** $p < 0.001$. (D) *IGF2* expression levels derived from fetal promoter P3 measured by quantitative RT-PCR in HCC samples with hypomethylation or normal methylation in fetal promoters (P3-P4). Fold change is normalized to 1 (mean expression value in healthy liver). Error bars are mean \pm SD in all panels. Statistical significance between groups is calculated Mann-Whitney test. * $p < 0.05$, ** $p < 0.01$, *** $p < 0.001$. (E) *IGF2* expression levels derived from adult promoter P1 measured by quantitative RT-PCR in HCC samples with normal methylation

or hypermethylation in P1. Fold change is normalized to 1 (mean expression value in healthy liver). Error bars are mean \pm SD. in all panels. Statistical significance between groups is calculated Mann-Whitney test. * $p < 0.05$, ** $p < 0.01$, *** $p < 0.001$. (F) *H19* levels determined by quantitative RT-PCR in HCC tumors and classified in low ($n = 194$) and high ($n = 34$) *IGF2* expression. Dots represent the expression value of each individual sample and the line is the mean value of each group. Fold change is normalized to 1 (mean expression value in healthy liver). Statistical significance between groups is calculated by Mann-Whitney test. ns; non-significant.

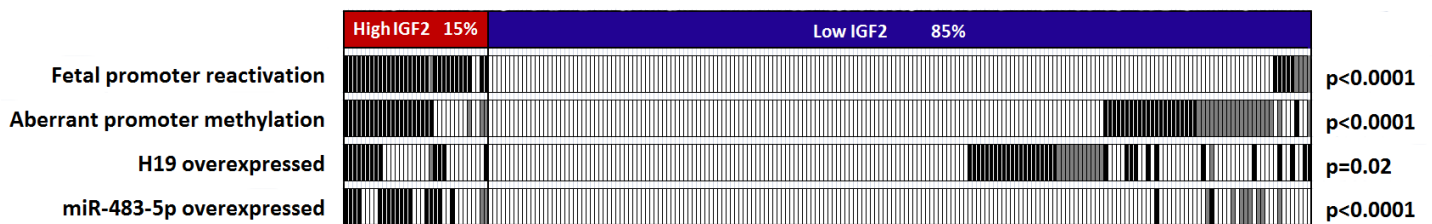


Supplementary Figure 4. Aberrant methylation pattern in *IGF2* promoters is associated with *IGF2* overexpression in HCC cell lines. (A) *IGF2* levels determined by quantitative RT-PCR in different human HCC cell lines. Fold change is normalized to 1 (mean expression value in healthy liver). Error bars are mean \pm SD. corresponding to ≥ 3 experiments in triplicate. (B) Representative Western Blot analysis of *IGF2* and consequent *IGF1R* and downstream pathway activation in HCC cell lines with high (Hep3B and Huh7) or low (PLC5 and SNU449) *IGF2* expression. Tubulin was used as a loading control. (C) Methylation levels measured by methylome array in CpGs of the maternal allele located within adult promoter (P1), fetal promoters (P3-P4) and the *IGF2/H19* imprinting locus (ICR1) in Hep3B (red; high *IGF2*) or SNU449 (blue; low *IGF2*) cells. Dots represent the mean value in each CpG. Fold change is normalized to 1 (mean expression value in healthy liver). (D) Methylation levels measured by methylome array in CpGs of the paternal allele located within adult promoter (P1), fetal promoters (P3-P4) and the *IGF2/H19* imprinting locus (ICR1) in Hep3B (red; high *IGF2*) or SNU449 (blue; low *IGF2*) cells. Dots represent the mean value in each CpG. Fold change is normalized to 1 (mean expression value in healthy liver). (E) *Left panel:* Methylated (black) and unmethylated (white) CpGs in P3 fetal promoter and P1 adult promoter in HCC cell lines with high (Hep3B, Huh7) and low (SNU449, PLC5) *IGF2* levels. Methylation status of CpGs was analyzed by bisulfite sequencing. *Right panel:* *IGF2* expression derived from P3 or P1 promoters determined by quantitative RT-PCR in human HCC cell lines. Error bars are mean \pm SD. corresponding to ≥ 3 experiments in triplicate.



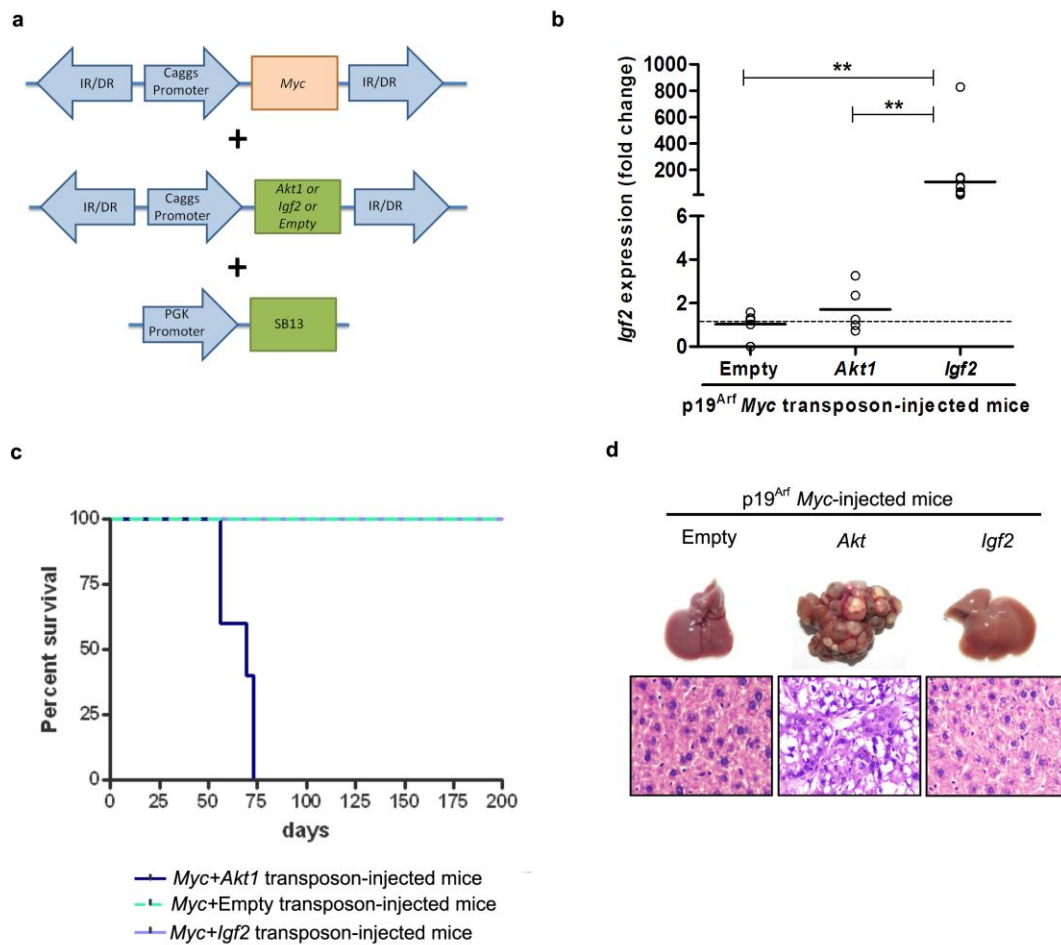
Supplementary Figure 5. Demethylation of *IGF2* fetal promoters leads to their reactivation and *IGF2* overexpression in HCC cell lines. (A) *Left panel:* Methylated (black) and unmethylated (white) CpGs in P3 fetal promoter in HCC cell lines with low *IGF2* levels (SNU449, PLC5) treated or not with 10 $\mu\text{mol/L}$ of the demethylating agent decitabine. Methylation status of CpGs was analyzed by bisulfite sequencing. *Right panel:* *IGF2* expression derived from P3 promoter determined by quantitative RT-PCR in human HCC cell lines with low *IGF2* levels (SNU449, PLC5) treated or not with 10 $\mu\text{mol/L}$ of the demethylating agent decitabine. (B) Expression of *miR-483-5p* measured by quantitative RT-PCR in SNU449 (left) or PLC5 (right) cells transfected with Mock miRNA or miR-483-5p. Fold change is normalized to 1 (mean expression value in the wild-type cell line). (C) Expression of *IGF2* measured by quantitative RT-PCR in SNU449 (left) or PLC5 (right) cells transfected with Mock miRNA or miR-483-5p. Fold change is normalized to 1 (mean expression value in the wild-type cell line).

Error bars are mean \pm SD. corresponding to ≥ 3 experiments in triplicate. Statistical significance between groups is calculated by two-sided t-test. * $p < 0.05$, ** $p < 0.01$, *** $p < 0.001$.



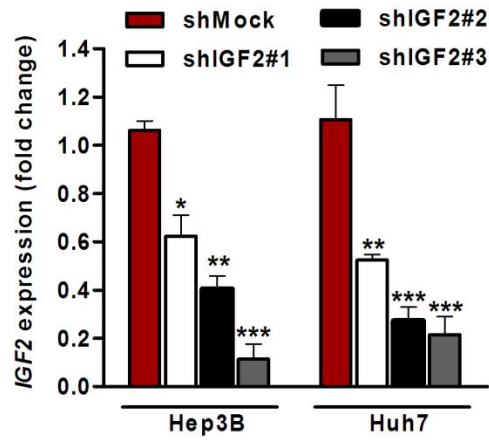
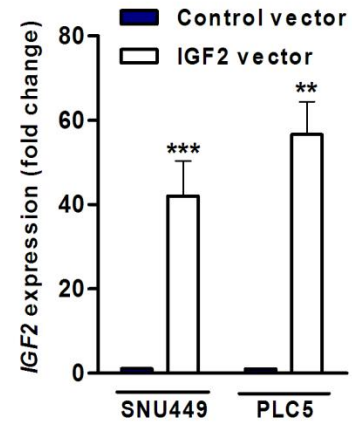
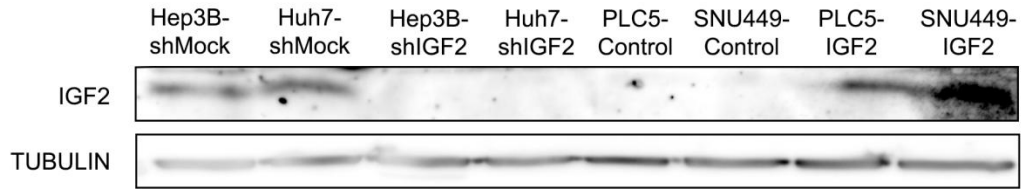
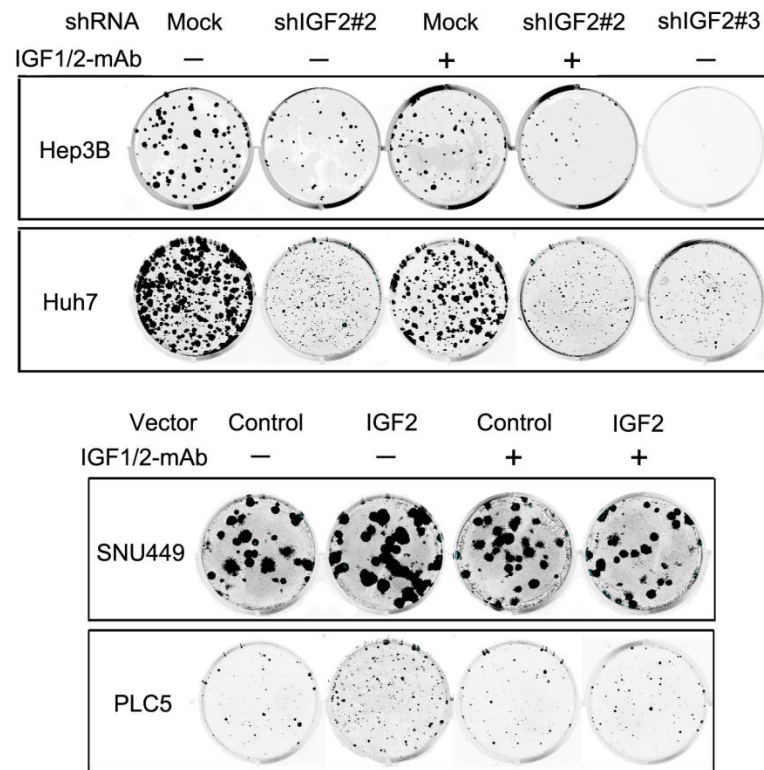
Supplementary Figure 6. Epigenetic deregulations affecting the 228 tumors in our cohort.

Overexpression of *IGF2* from fetal promoters, as well as aberrant promoter methylation, and H19 and miR-483-5p overexpression, were all significantly associated with IGF2 overexpression ($p < 0.0001$ in all cases, except for H19 which was $p = 0.02$). Statistical significance is calculated by χ^2 test.

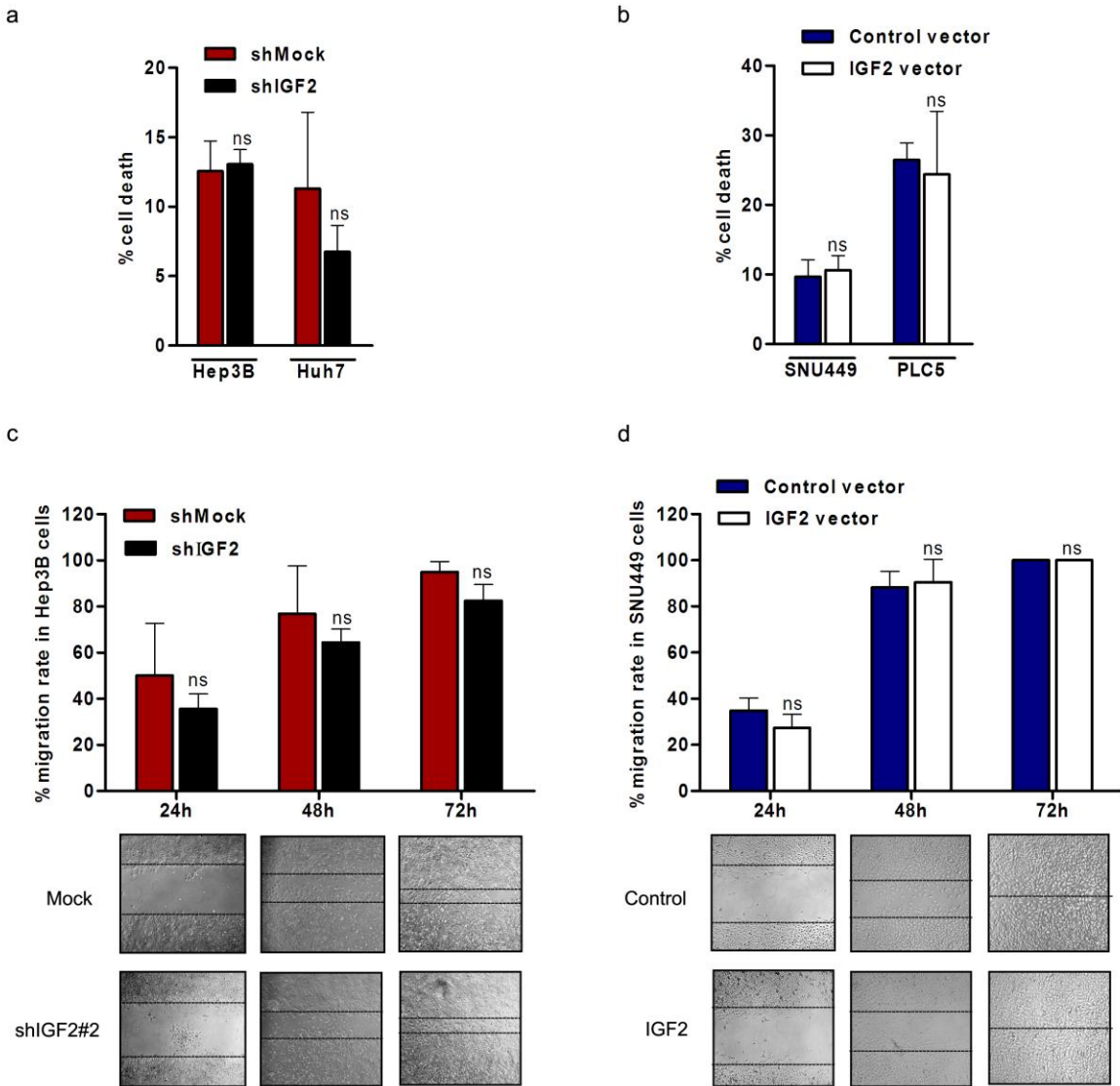


Supplementary Figure 7. *Igf2* overexpression alone is not able to initiate hepatocarcinogenesis in *in vivo* models. (A) Schematic representation of transposable elements encoding *Myc* and *Igf2*, *Akt1* or an Empty vector. Caggs, CAGGS promoter; IR/DR, inverted repeats and direct repeats; IRES, internal ribosome entry site. (B) *Igf2* expression levels measured by qRT-PCR in livers upon intrahepatic delivery of *Myc*+Empty vector (Negative Control; $n = 5$), *Myc*+*Akt1* (Positive control; $n = 6$) and *Myc*+*Igf2* ($n = 6$). Dots represent the expression value of each individual sample and line is the mean value of each group. Fold change is normalized to 1 (mean expression value in

livers of Negative control-transposon injected mice). Statistical significance between groups is calculated by Kruskal-Wallis with Dunn's multiple comparison test. * $p < 0.05$, ** $p < 0.01$, *** $p < 0.001$. (C) Survival analysis (Kaplan-Meier) of p19^{Arf^{-/-}} mice upon intrahepatic delivery of *Myc*+Empty vector (Negative Control; $n = 5$), *Myc*+*Akt1* (Positive control; $n = 6$) and *Myc*+*Igf2* constructs ($n = 6$). For survival analysis, mice were censored at the time of sacrifice according to IACUC guidelines. Statistical significance between groups is calculated by log-Rank test. (D) Representative images and H&E staining of intrahepatic tumor burden 200 days after delivery of *Myc*+Empty vector, *Myc*+*Akt* or *Myc*+*Igf2* into livers of p19^{Arf^{-/-}} mice.

a**b****c****d**

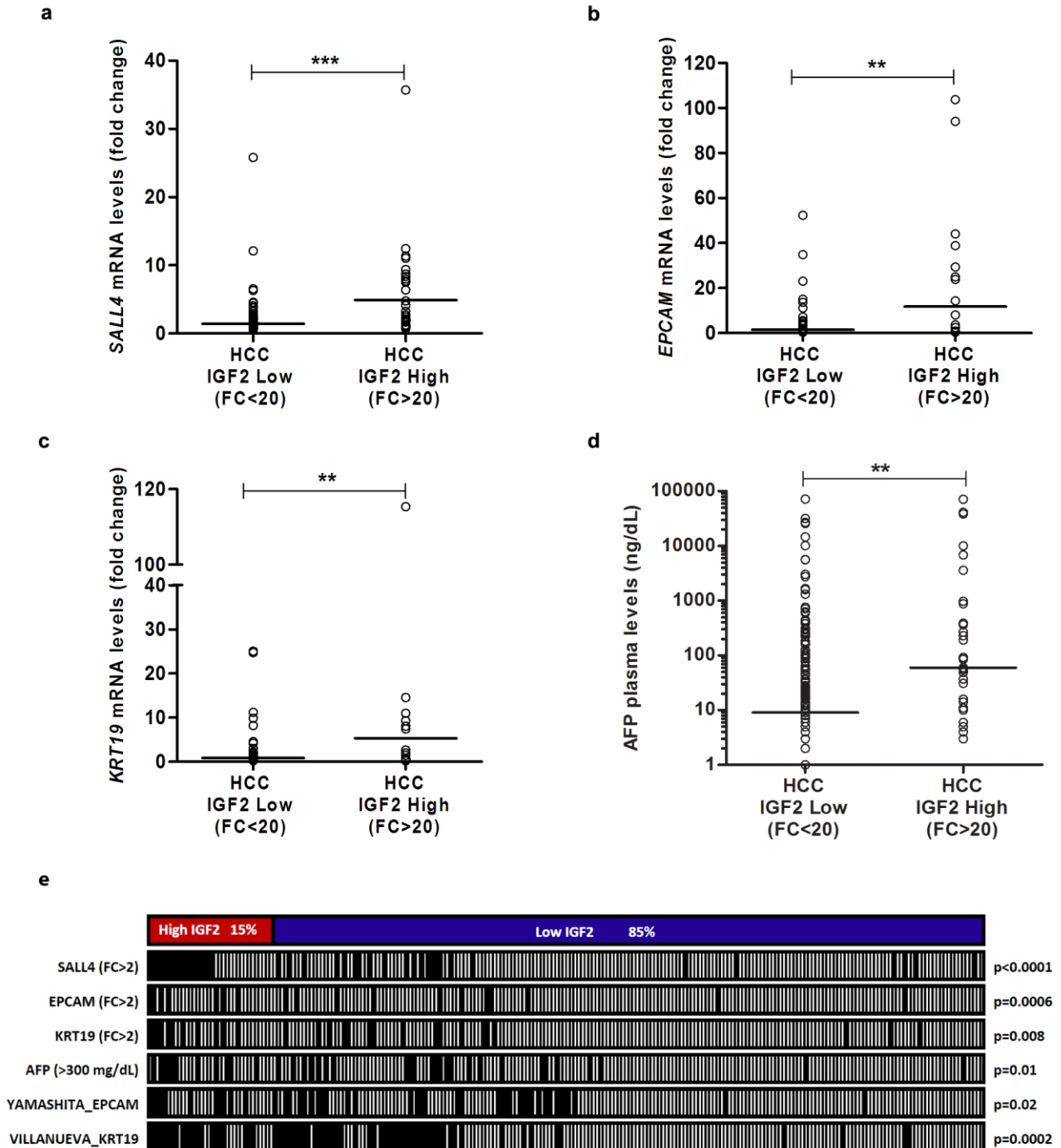
Supplementary Figure 8. Effects of IGF2 on HCC cell proliferation. (A) Expression of *IGF2* measured by quantitative RT-PCR in Hep3B (left) or Huh7 (right) cells stably transfected with Mock shRNA or three different shIGF2. Fold change is normalized to 1 (mean expression value in the wild-type cell line). Statistical significance between groups is calculated by one-way ANOVA with post-hoc Bonferroni test. * $p < 0.05$, ** $p < 0.01$, *** $p < 0.001$. (B) Expression of *IGF2* measured by quantitative RT-PCR in SNU449 (left) or PLC5 (right) cells stably transfected with a Control vector or an IGF2-overexpression vector. Fold change is normalized to 1 (mean expression value in the wild-type cell line). Statistical significance between groups is calculated by one-way ANOVA with post-hoc Bonferroni test. * $p < 0.05$, ** $p < 0.01$, *** $p < 0.001$. (C) Representative Western Blot analysis of IGF2 in cells stably transfected with Mock shRNA or a shIGF2 (Hep3B and Huh7) and cells stably transfected with a Control vector or an IGF2-overexpression vector (PLC5 and SNU449). Tubulin was used as a loading control. (D) Representative image of a colony formation assay (crystal violet staining) using Hep3B or Huh7 cell lines stably transfected with Mock shRNA or two different shIGF2, and treated with the IGF1/2-mAb (*upper panel*) or SNU449 or Huh7 cell lines stably transfected with a Control vector or a IGF2-overexpression construct, and treated with IGF1/2-mAb (*lower panel*).



Supplementary Figure 9. IGF2 has no effect in cell death and migration of HCC cells.

(A) Percentage of cell death measured by FACS in Hep3B (left) or Huh7 (right) cells stably transfected with Mock shRNA or a shIGF2. (B) Percentage of cell death measured by FACS in SNU449 (left) or PLC5 (right) cells stably transfected with a Control vector or an IGF2-overexpression construct. (C) *Upper panel*: Migration rates in Hep3B-Mock and Hep3B-shIGF2 are represented as the percentage of the initial wound surface covered by cells 24, 48 and 72h after injury. *Lower panel*: representative images of each time point of

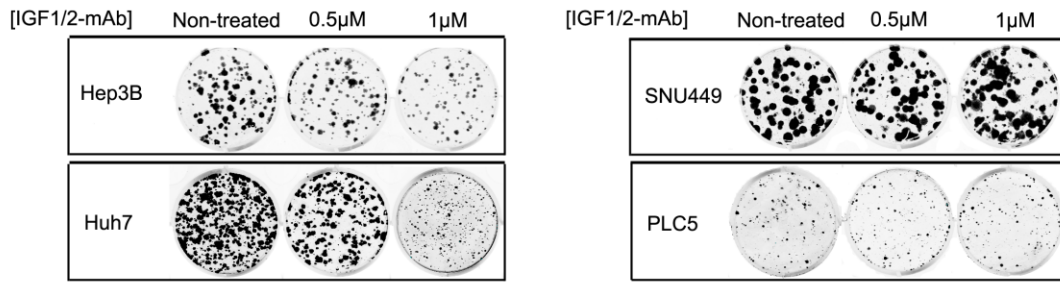
the migration assay. **(D)** *Upper panel*: Migration rates in SNU449-Control vector and SNU449-IGF2 24, 48 and 72h after injury. *Lower panel*: representative images of each time point of the experiment. Error bars are mean \pm SD. corresponding to ≥ 3 experiments in triplicate. Statistical significance between groups is calculated by two-sided t-test. ns, non-significant.



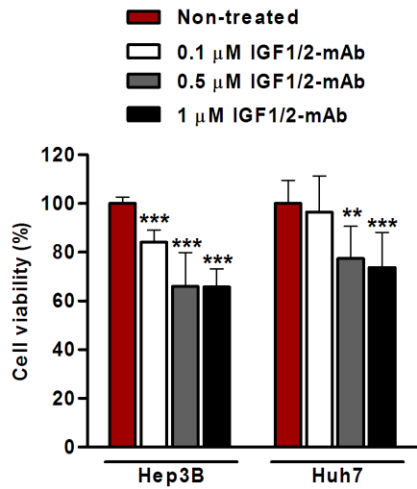
Supplementary Figure 10. Upregulation of hepatic progenitor cell markers and increased plasma AFP levels are associated with *IGF2* re-expression in HCC. (A) *SALL4*, (B) *EPCAM* and (C) *KRT19* mRNA levels were determined by expression array and (D) Alpha fetoprotein levels (AFP) were detected in plasma of HCC patients with low

($n = 194$) and high ($n = 34$) *IGF2* tumor expression. Dots represent the expression value of each individual sample and the line is the mean value of each group. Fold change is normalized to 1 (mean expression value in healthy liver). Statistical significance between groups is calculated by Mann-Whitney test. * $p < 0.05$, ** $p < 0.01$, *** $p < 0.001$. **(E)** Schematic representation of the overexpression (defined as >2 fold) of hepatic progenitor markers SALL4, EPCAM and KRT19; high plasma levels of alpha fetoprotein (AFP; defined as >300 ng/dL); and genomic signatures of EPCAM²⁴ and KRT19²⁵ markers associated with IGF2 reactivation. Statistical significance is calculated by χ^2 test.

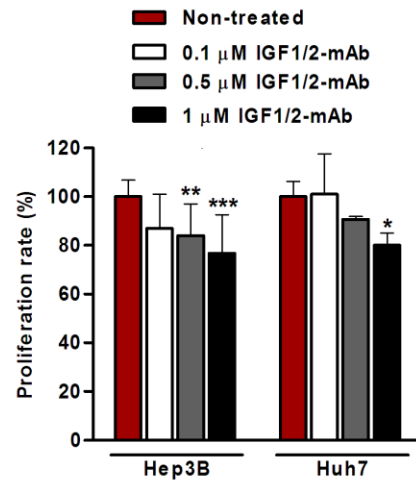
a



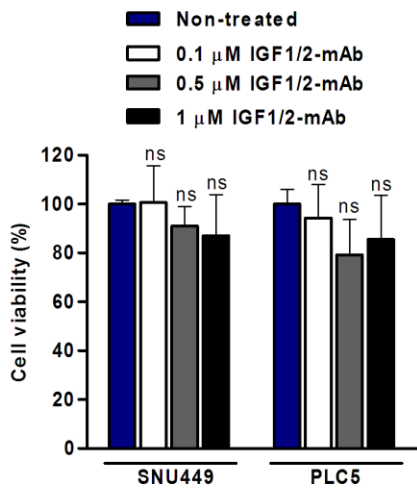
b



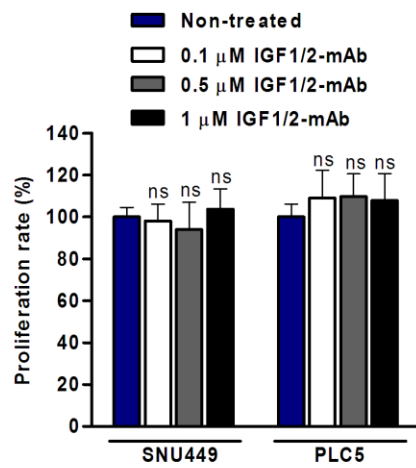
c



d

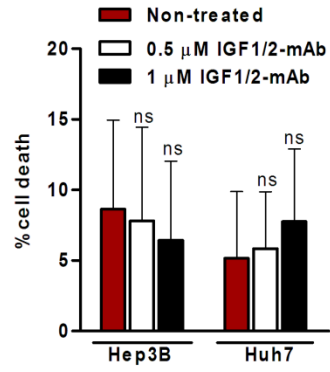


e

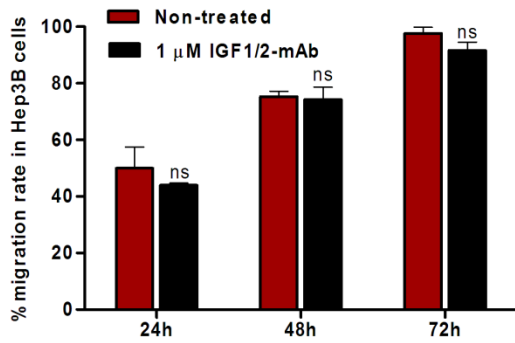


Supplementary Figure 11. Anti-proliferative effects of IGF1/2-mAb in HCC cell lines overexpressing IGF2. (A) Representative image of a colony formation assay (crystal violet staining) using Hep3B and Huh7 cell lines (high IGF2) or SNU449 and PLC5 (low IGF2) cell lines treated with different concentrations of IGF1/2-mAb. (B) Cell viability of Hep3B and Huh7 cell lines (high IGF2) treated with IGF1/2-mAb for 48h at different concentrations. (C) Cell proliferation rate of Hep3B and Huh7 cell lines (high IGF2) treated with IGF1/2-mAb for 48h at different concentrations. (D) Cell viability of SNU449 and PLC5 cell lines (low IGF2) treated with IGF1/2-mAb for 48h at different concentrations. (E) Cell proliferation rate of SNU449 and PLC5 cell lines (low IGF2) treated with IGF1/2-mAb for 48h at different concentrations. Error bars are the percentage normalized to non-treated control \pm SD. corresponding to ≥ 3 experiments in triplicate. Statistical significance between groups is calculated by one-way ANOVA with post hoc Bonferroni test. * $p < 0.05$, ** $p < 0.01$, *** $p < 0.001$, ns; non-significant.

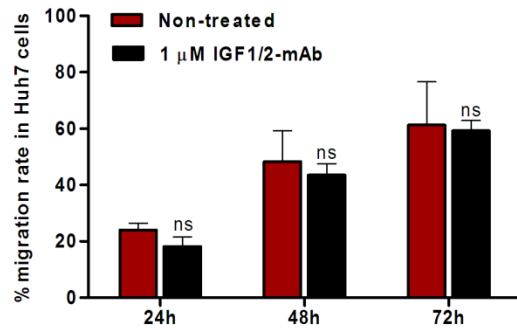
a



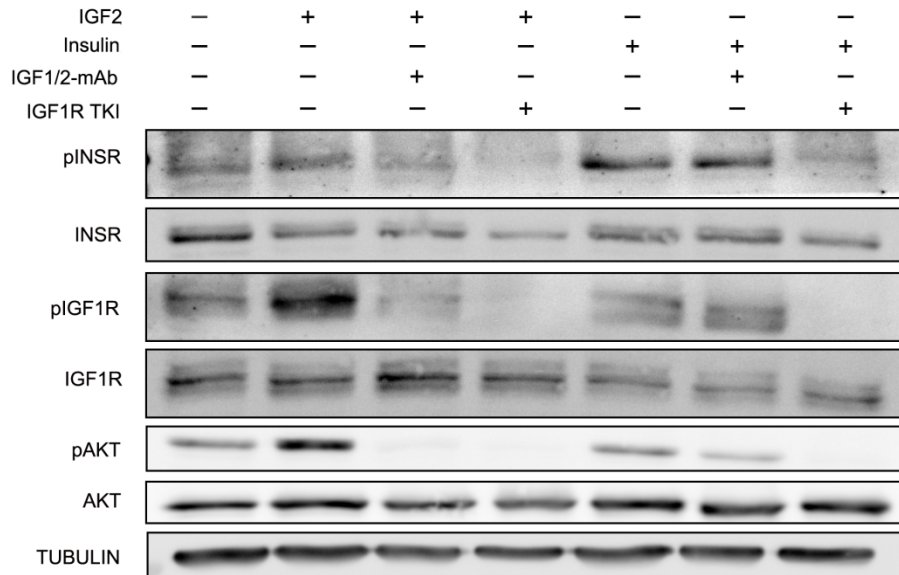
b



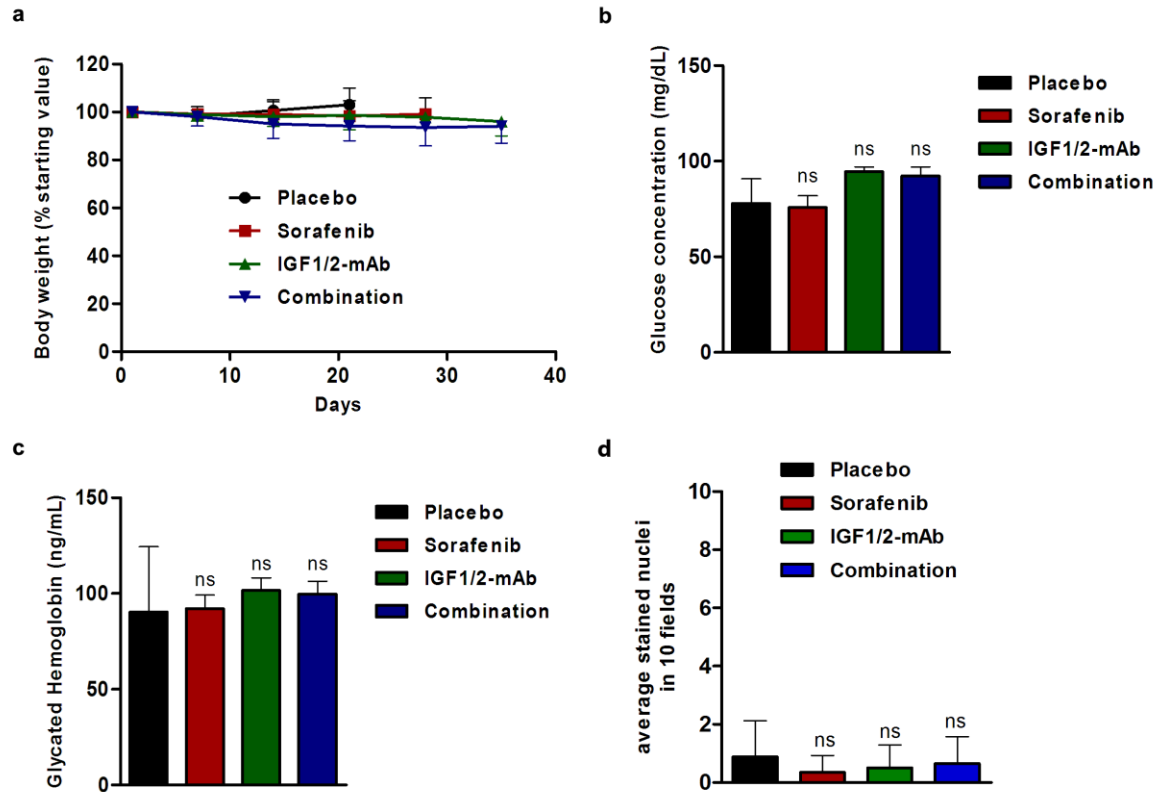
c



d



Supplementary Figure 12. IGF1/2-mAb has no effects in cell death and migration of HCC cells. (A) Percentage of cell death measured by FACS in Hep3B (left) or Huh7 (right) cells treated with 1 $\mu\text{mol/L}$ of IGF1/2-mAb. (B) *Upper panel:* Migration rates in Hep3B treated or not with 1 $\mu\text{mol/L}$ of IGF1/2-mAb are represented as the percentage of the initial wound surface covered by cells 24, 48 and 72h after injury. *Lower panel:* representative images of each time point of the migration assay. (C) *Upper panel:* Migration rates in Huh7 treated or not with 1 $\mu\text{mol/L}$ of IGF1/2-mAb are represented as the percentage of the initial wound surface covered by cells 24, 48 and 72h after injury. *Lower panel:* representative images of each time point of the migration assay. Error bars are mean \pm SD, corresponding to ≥ 3 experiments in triplicate. Statistical significance between groups is calculated by two-sided t-test. ns, non-significant. (D) Representative Western Blot analysis of Huh7 (high *IGF2*) cells stimulated by IGF2 or Insulin and treated with IGF1R TKI or IGF1/2-mAb for 15 min. Tubulin was used as a loading control.



Supplementary Figure 13. IGF1/2-mAb and its combination with sorafenib are well tolerated in HCC xenograft model. (A) Mean mice body weight in each treatment group over time. (B) Glucose levels on tail vein blood measured after three weeks of treatment. (C) Concentration of glycated hemoglobin in whole blood samples assessed before sacrifice. (D) Quantification of apoptosis events by TUNEL assay in 10 fields (40x magnification). Statistical significance between vehicle ($n = 8$), sorafenib ($n = 13$), IGF1/2-mAb ($n = 12$) and combination ($n = 13$) is calculated by one-way ANOVA with post hoc Bonferroni test. ns, non-significant.

Supplementary Materials and Methods

Genomic profiling and data analysis

All samples used for the genomic profiling were fresh-frozen. RNA and DNA were extracted as previously described⁷. Human and mouse transcriptomic profiling were conducted using the Human Genome U219 Array Plate (Affymetrix, Santa Clara, CA) and the MouseWG-6 v2.0 (Illumina, San Diego, CA), respectively. mRNA levels were additionally measured by quantitative RT-PCR. miRNA profiling of 218 samples was conducted using the GeneChip miRNA 2.0 Array (Affymetrix).

Processing of transcriptome data (i.e., normalization, background correction, and filtering) was conducted as previously reported.²⁵ Genes and miRNAs differentially expressed in HCC tumors with high levels of *IGF2* (>20-fold, FDR<0.05 in human samples; >2-fold, FDR<0.05 in cell lines) were identified through the Comparative Marker Selection module of Gene Pattern (www.broadinstitute.org), and later submitted to Ingenuity Pathway Analysis (IPA) (www.ingenuity.com). To provide further biological insight on samples with high *IGF2* levels, we used the Nearest Template Prediction (NTP) and Gene Set Enrichment Analysis (GSEA) modules of Gene Pattern. All gene signatures analyzed were already reported in the Molecular Signature Database (www.broadinstitute.org/gsea/msigdb). Microarray data were deposited in Gene Expression Omnibus database with the accession numbers GSE63898, GSE56588, GSE74618 and GSE85274.

Methylome profiling

Methylome profiling and data analysis from the human cohort and HCC cell lines was performed by using the Illumina Methylation platform 450K as previously described.⁷ To study the differential methylation in *IGF2* between HCC and normal liver tissue, we used array probes located at the fetal (P3-P4) and adult (P1) promoters of the *IGF2* gene and the ICR1 (CTCF-binding site) according to Ensembl Genome Browser (Ensembl.org). Methylation probes located within the ICR1 and *IGF2* promoters are listed in the **Table S2**. Hypomethylation and hypermethylation were defined as the mean fold-change compared to healthy liver samples ± 2 SD.

Additionally, DNA methylation in HCC cell lines was evaluated through bisulfite conversion sequencing. 500 ng of DNA were converted using the EpiTect® Fast DNA Bisulfite Kit (Qiagen, Valencia, CA), following the manufacturer's recommendations. Primer sets for PCR amplification and sequencing are summarized in **Table S3**. PCRs were performed under standard conditions, PCR products were sequenced by Sanger (Beckman Coulter Inc, Brea, CA) and results were analyzed using the Mutation Surveyor® software (SoftGenetics, State College, PA).

Decitabine demethylation treatment

PLC5 and SNU449 cell lines were treated with 10 μ mol/L of decitabine (Sigma, St. Louis, MO) for 96h adding fresh drug daily. After 96h, DNA and RNA were extracted as previously described⁷ and methylation status of *IGF2* promoters and mRNA *IGF2* expression was assessed.

Cell lines, plasmids and reagents

Hep3B, HepG2, SNU182, SNU387, SNU423, SNU398, SNU449 and PLC5 cell lines were obtained from the ATCC, while the Huh7 cell line was purchased from the Japanese Collection of Research Bioresources. Cell lines were regularly confirmed to be mycoplasma free using EZ-PCR kit (Biological Industries, Kibbutz Beit Haemek, Israel). HCC cell lines were cultured in DMEM or RPMI (ThermoFisher, Waltham, MA) supplemented with 10% heat-inactivated fetal bovine serum (FBS). SNU449 and PLC5 cell lines stably expressing *IGF2* were generated by transfecting 5 µg of EX-Z6323-M14 vector containing human *IGF2* ORF (NM_001127598.1) and a G418-selection cassette (GeneCopoeia™, Rockville, USA). The Hep3B and Huh7 cell lines were stably transfected with 5 µg of psi-H1 vector containing the shIGF2#1,2 or 3 (**Table S4**), a Puromycin-selection cassette and a eGFP reporter gene (GeneCopoeia™). Cells were transfected using Lipofectamine 3000® (ThermoFisher), and 48h after transfection cells were selected with G418 (1 mg/ml, G418 disulfate salt (Sigma) or Puromycin (1 µg/ml, Puromycin dihydrochloride (Sigma)). BI836845 (IGF1/2-mAb) humanized monoclonal antibody was provided by Boehringer Ingelheim (Vienna, AT), whereas sorafenib and linsitinib (IGF1R TKI) were purchased from LC Laboratories (Woburn, MA, USA) and BioVision (Milpitas, CA, USA), respectively.

miRNAs transfection

SNU449 and PLC5 cell lines expressing miR-483-5p were generated by transfecting 100nM of miRIDIAN microRNA Human hsa-miR-483-5p mimic or miRIDIAN microRNA Mimic Negative Control #1 (Dharmacon). Cells were transfected using

DharmaFECT Transfection Reagent (Dharmacon), and 72 hours after transfection RNA was extracted using the miRNeasy mini kit (Qiagen).

cDNA was synthesized from 5ng of total RNA in 15 μ l reaction using miRNA-specific primers and the TaqMan[®] MicroRNA Reverse Transcription Kit (Applied Biosystems) according to manufacturer's instructions. High Capacity cDNA reverse Transcription kit (Applied biosystems) was used to synthesize cDNA for gene expression assays. For relative miRNA quantification, TaqMan[®] Gene Expression Assays were used following the manufacturer's instructions (Applied Biosystems). TaqMan[®] probes are listed in **Table S5**. miR-23b was chosen as the endogenous reference miRNA.

Reverse transcription Polymerase Chain Reaction (PCR) and quantitative RT-PCR

Total RNA was extracted either from cells collected at 80% confluence or from tissue, using the RNeasy Mini Kit (Qiagen). 1 μ g of RNA was retrotranscribed to cDNA using the High-Capacity cDNA Reverse Transcription Kit (Applied Biosystems, Waltham, MA). For relative mRNA quantification, TaqMan[®] Gene Expression Assays were used following the manufacturer's instructions (Applied Biosystems). TaqMan[®] probes are listed in **Table S5**. Ribosomal RNA (*18S*) was chosen as the endogenous reference gene. Specific methods and TaqMan probes used for *INSR-A* gene expression assays were described in detail in Huang *et al.* (58).

***In vitro* functional cell assays**

For the cell viability assay, cells were seeded in 96-well plates and incubated with increasing concentrations (0 μ mol/L, 0.1 μ mol/L, 0.5 μ mol/L or 1 μ mol/L) of the IGF1/2-

mAb for 48 h in humidified atmosphere at 37°C and 5% CO₂. Cell viability was determined by 3-(4,5-dimethylthiazol-2-yl)-2,5-diphenyltetrazolium bromide (MTT) dye uptake using the CellTiter 96® Cell Proliferation Kit (Promega, Madison, WI) following the manufacturer's instructions. To assess proliferation, BrdU (bromodeoxyuridine) incorporation into newly synthesized DNA was measured by BrdU Cell Proliferation Assay Kit (Cell Signaling, Danvers, MA). For the colony formation assay, 200-1000 cells/well were seeded in 6-well plates and incubated for 2 weeks in the presence of 0 μM, 0.5 μM or 1 μM of IGF1/2-mAb. Thereafter, cells were stained with 0.5% Crystal Violet (Sigma) and the number of colonies and colony size was measured using Odyssey CLx Infrared Imaging System (Li-Cor, Lincoln, NE). To determine cell death, cells were seeded in 10 cm Petri dishes and maintained in FBS-free media for 24 h. Cells were treated either with 0 μM or 1 μM of IGF1/2-mAb. 48 h after treatment, cells were collected and fixed overnight at -20 °C using ice-cold 70%-ethanol, and stained with propidium iodide. Cell death was evaluated by determining the subG0 population on a BD FACS Canto II flow cytometer (Becton Dickinson, Franklin Lakes, NJ). Migration was assessed using the wound healing assay in cells treated with 0 μM or 1 μM of IGF1/2-mAb in the presence of mitomycin C (Sigma). Cell migration rate was evaluated at several time points by measuring the percentage of the initial wound area covered by cells over time on microscope images (ImageJ software).

IGF2 immunostaining

IGF2 immunohistochemistry was done on 5-μm sections of FFPE blocks using the anti-IGF2 antibody from Abcam (ab9574) Antigen retrieval was performed in citrate buffer using a microwave oven. After antigen retrieval, samples were incubated with peroxidase and blocked with Antibody Diluent containing Background Reducing Component (Dako,

Golstrup, Denmark). Sections were incubated O/N at 4°C with anti-IGF2 antibodies (1:400). EnVision™+ System-HRP (DAB) was applied as secondary antibody (Dako, Golstrup, Denmark). Samples were counterstained with hematoxylin.

Ligand mediated IGF pathway activation

Cells were seeded in 10 cm Petri dishes and incubated with FBS-free media overnight. IGF pathway activation was done by treating cells with 100 nM of IGF2 or 60 ng/ml of insulin (Preprotech, Rocky Hill, NJ) and inhibition, by applying 1 µM of IGF1/2-mAb (BI 836845) or 35 nM of IGF1R TKI (linsitinib) for 15min. IGF2 expression and pathway activation were analyzed by Western Blot. In short, cells were lysed in lysis buffer (50 mM Tris pH=7.4, 150 mM NaCl, 1% Triton X-100, 0.1% SDS, 0.25 mM EDTA, 1% Sodium deoxycholate) containing protease and phosphatase inhibitors. 60 µg of protein were resolved by electrophoresis and transferred to nitrocellulose membranes (ThermoFisher). Membranes were incubated overnight at 4 °C with IGF2 (ab9574), phosphoINSR(#3023), INSR(#3025), phosphoIGF1R (#6113), IGF1R (#3027), phosphoAKT (#9271) and AKT (#9272) antibodies (Cell Signaling), followed by incubation with HRP-linked secondary antibodies (Agilent Technologies, Santa Clara, CA). The HRP signal was used as a surrogate protein and was quantified through LAS4000 imaging and ImageGauge.v4 software (Fujifilm, Tokyo, Japan).

Metabolic toxicity in the HCC subcutaneous xenograft mouse model

Blood glucose levels were assessed after three weeks of treatment by using the ACCU-CHEK Sensor Confort test strips on tail vein blood (Roche, Basel, Switzerland). To evaluate glycated hemoglobin (hemoglobin A1c) whole blood samples were collected after

cardiac puncture immediately prior to euthanasia. GHbA1c ELISA Kit (Neobiolab, Woburn, MA) was used to measure the concentration of glycosylated hemoglobin.

Tumor xenograft molecular characterization

To evaluate cell proliferation and microvessel density, 4 µm sections of paraffin-embedded tumors were immunostained with Ki-67 and CD31 antibodies (Agilent Technologies). Ki-67 staining was quantified as the number of Ki-67 immunopositive cells divided by the total number of cells per field. Apoptosis was evaluated using the DeadEnd™ Colorimetric TUNEL System (Promega, Wisconsin, WI). Number of cells positively stained in the TUNEL assay was scored in ten microscopic fields. Microvessel density was determined by measuring the area of CD31 positive blood vessels. In all cases 10 randomly selected fields were quantified (40x and 20x, respectively). Images were produced using a Axioskop-2 microscope (Zeiss, Oberkochen, Germany). Phosphorylation of IGF1R, AKT and ERK was assessed by Western Blot. *Vegfa* gene expression was measured by TaqMan® Gene Expression Assays (Applied Biosystems).

***Igf2* and *H19* expression analysis in mouse models of HCC**

Expression of *Igf2* and *H19* was assessed by qRT-PCR in tumors from our chemically-induced mouse model of HCC and by microarray in 10 expression datasets from different mouse models of HCC publicly available in Gene Expression Omnibus database (<http://www.ncbi.nlm.nih.gov/geo/>): GSE33486, GSE2127, GSE31431, GSE15251, GSE26538, GSE39401, GSE19004, GSE46646, GSE54054, GSE61422. A FC>2 compared to healthy liver tissue in control mice was considered as overexpression for both genes.